



Original article

Synthesis, anticancer activity and QSAR study of 1,4-naphthoquinone derivatives



Veda Prachayasittikul^a, Ratchanok Pingaew^b, Apilak Worachartcheewan^c,
Chanin Nantasenamat^c, Supaluk Prachayasittikul^{c,*}, Somsak Ruchirawat^{d,e,f},
Virapong Prachayasittikul^{a,*}

^a Department of Clinical Microbiology and Applied Technology, Faculty of Medical Technology, Mahidol University, Bangkok 10700, Thailand

^b Department of Chemistry, Faculty of Science, Srinakharinwirot University, Bangkok 10110, Thailand

^c Center of Data Mining and Biomedical Informatics, Faculty of Medical Technology, Mahidol University, Bangkok 10700, Thailand

^d Laboratory of Medicinal Chemistry, Chulabhorn Research Institute, Bangkok 10210, Thailand

^e Program in Chemical Biology, Chulabhorn Graduate Institute, Bangkok 10210, Thailand

^f Center of Excellence on Environmental Health and Toxicology, Commission on Higher Education (CHE), Ministry of Education, Thailand

ARTICLE INFO

Article history:

Received 11 April 2014

Received in revised form

26 June 2014

Accepted 5 July 2014

Available online 9 July 2014

Keywords:

Anticancer

1,4-Naphthoquinone derivatives

QSAR

Structural modification

ABSTRACT

A series of 2-substituted amino-3-chloro-1,4-naphthoquinone derivatives (**3–12**) were synthesized as anticancer agents and tested against four cancer cell lines including HepG2, HuCCA-1, A549 and MOLT-3. The most potent cytotoxic activity against the HepG2, HuCCA-1 and A549 cell lines was found to be *m*-acetylphenylamino-1,4-naphthoquinone (**8**) affording IC₅₀ values of 4.758, 2.364 and 12.279 μM, respectively. On the other hand, *p*-acetylphenylamino-1,4-naphthoquinone (**9**) exhibited the most potent cytotoxic activity against the MOLT-3 cell line with an IC₅₀ of 2.118 μM. Quantitative structure–activity relationship (QSAR) investigations provided good predictive performance as observed from cross-validated *R* of 0.9177–0.9753 and RMSE of 0.0614–0.1881. The effects of substituents at the 2-amino position on the naphthoquinone core structure and its corresponding influence on the cytotoxic activity were investigated by virtually constructing additional 1,4-naphthoquinone compounds (**13–36**) for which cytotoxic activities were predicted using equations obtained from the previously constructed QSAR models. Interpretation of informative descriptors from QSAR models revealed pertinent knowledge on physicochemical properties governing the cytotoxic activities of tested cancer cell lines. It is anticipated that the QSAR models developed herein could provide guidelines for further development of novel and potent anticancer agents.

© 2014 Published by Elsevier Masson SAS.

1. Introduction

There is a continual increase on the incidence of cancer and it is considered to be the leading cause of morbidity and mortality [1]. Recently, considerable attention has been drawn on the search for novel anticancer drugs in order to improve survival rates and well-being.

The quinone scaffold is presented in many currently used anticancer drugs [2,3]. Particularly, 1,4-naphthoquinones are active quinone derivatives that are widely used as raw materials in pharmaceuticals and agrochemicals industries. A diverse array of

bioactivities has been reported for 1,4-naphthoquinone derivatives to exert anticancer [2,4–8], antimicrobial [9–12], antifungal [10,13–15], antiviral [11,16–18], radical scavenging [19], antiplatelet [20–22] and trypanocidal [23] activities.

1,4-Naphthoquinone contains two ketone groups as a crucial chromophore that accounts for its bioactivities owing to their ability to accept electrons [24]. Structure–activity relationship study indicated that cytotoxic activity of 1,4-naphthoquinones are closely related with their electron accepting capability [25], which gives rise to reactive oxygen species (ROS) production leading to DNA damage and cell death [2,25,26]. Furthermore, enhanced antimicrobial activity was reported in amino derivatives of 1,4-naphthoquinone [13,27]. The findings indicated that the nitrogen atom of the amino substituent could improve the redox potential of the quinone system [25,28]. In addition, insertion of a chlorine substituent into the amino derivative of 1,4-naphthoquinone

* Corresponding authors.

E-mail addresses: supaluk@swu.ac.th (S. Prachayasittikul), virapong.pra@mahidol.ac.th (V. Prachayasittikul).

nucleus was found to improve the redox potential of compounds while not significantly affecting their hydrophobicities [25].

Besides the mechanism of ROS production, cytotoxic effect of clinically used quinone-based anticancer drugs are closely related to an inhibition of DNA topoisomerase II enzyme [3,29]. The DNA topoisomerase II is an essential enzyme required for DNA replication, chromosome condensation and chromosome segregation [3,30]. DNA unwinding process is a crucial step in which the coils of double stranded DNA needs to be uncoiled thereby allowing further processes of DNA replication [3].

In silico approaches play an important role in drug design and development. Quantitative structure–activity relationship (QSAR) is a computational method for correlating chemical structures of compounds with their respective biological activities [31–35]. Furthermore, QSAR studies could provide crucial pharmacokinetic information such as absorption, distribution, metabolism and excretion [36] which are important parameters in drug design and development.

Herein, a series of 2-amino-1,4-naphthoquinone derivatives (**3–12**, Fig. 1) were synthesized using the nucleophilic displacement reaction of 2,3-dichloro-1,4-naphthoquinone (**1**) by amines (**2**) as shown in Scheme 1 and subsequently investigated for their cytotoxic activity against four human cancer cell lines i.e. HepG2, HuCCA-1, A549 and MOLT-3. The resulting experimental data were consequently used for QSAR analysis. In order to elucidate the effect of 2-substituted amino group on the 1,4-naphthoquinone scaffold, an additional set of 24 structurally modified compounds with alkylamino, phenylamino and quinolinylamino substituents (**13–36**, Fig. 2) were virtually constructed and their pIC_{50} values were predicted from the QSAR models.

2. Results and discussion

2.1. Chemistry

A series of 2-amino-3-chloro-1,4-naphthoquinones (**3–12**) were synthesized *via* the nucleophilic substitution reaction of 2,3-dichloro-1,4-naphthoquinone (**1**) by appropriate primary and secondary amines (**2**) in refluxing ethanol (Scheme 1).

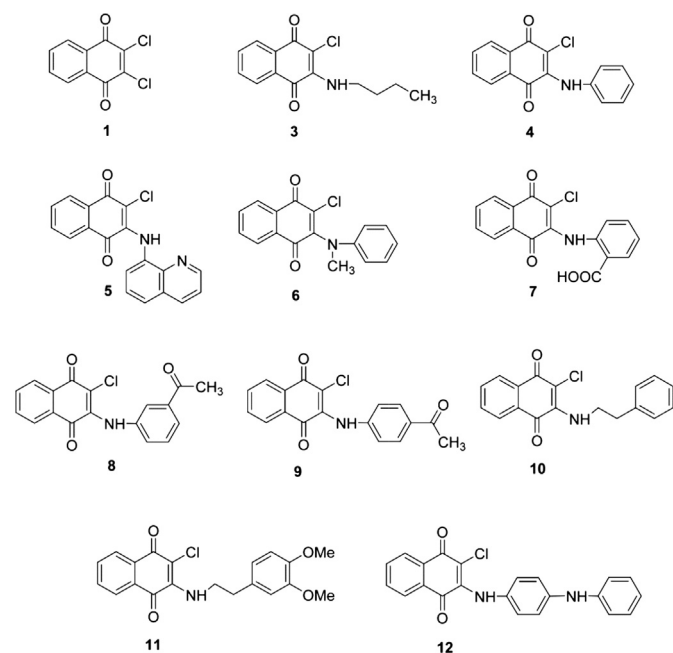


Fig. 1. Chemical structures of compounds **1** and **3–12**.

The aminoquinones (**3–12**) were obtained in 26–65% yields as dark orange, crimson and dark green solid. Structures of the quinone derivatives were confirmed by spectroscopic methods comprising of 1H and ^{13}C NMR, IR and HRMS. For example, spectral data of compound **3** are given. In the HRMS–TOF, the molecular ion $[M+H]^+$ peak of compound **3** was observed at 264.0783 corresponding to its molecular formula of $C_{14}H_{15}ClNO_2$. The IR spectra of compound **3** revealed absorption bands of N–H group at 3304 cm^{-1} and of C=O moiety at 1683 cm^{-1} . The 1H NMR spectra exhibited a triplet of methyl proton at δ 0.90 ppm with J value of 7.3 Hz. Three methylene protons of amino side chain appeared at δ 1.33 ppm as a sextet ($J = 7.3$ Hz), δ 1.59 ppm as a quintet ($J = 7.3$ Hz) and δ 3.72 ppm as a triplet ($J = 7.3$ Hz). The broad singlet at δ 7.51 ppm was assigned to the NH proton. In addition, four aromatic protons of naphthoquinone ring displayed at 7.73 (t, $J = 7.4$ Hz, 1H), 7.82 (t, $J = 7.5$ Hz, 1H), 7.97 (d, $J = 7.7$ Hz, 2H). In the ^{13}C NMR spectra, characteristic signals of two carbonyl carbons of naphthoquinone were visible at chemical shift 175.8 and 180.7 ppm.

2.2. Cytotoxic activity

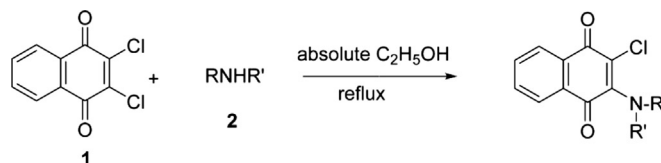
Cytotoxic activities of the synthesized aminoquinone compounds (**3–12**) and parent compound (**1**) were tested against four human cancer cell lines and normal embryonic lung cells (MRC-5) using etoposide and doxorubicin as reference drugs (Table 1). Compounds at 50 $\mu\text{g/mL}$ exhibiting less than 50% inhibition were considered to be inactive whereas ones exhibiting greater than 50% inhibition were considered to be active and their IC_{50} values were calculated. Compounds **1** and **3–12** were categorized by their cytotoxic activities as highly active ($IC_{50} < 1\ \mu\text{M}$), moderately active ($1\ \mu\text{M} < IC_{50} < 10\ \mu\text{M}$), weakly active ($IC_{50} > 10\ \mu\text{M}$) [37] and inactive ($IC_{50} > 50\ \mu\text{g/mL}$) as shown in Table 1.

Among all the tested compounds, acetylphenylaminoquinone compounds (**8** and **9**) were shown to be the most active compounds against all cancer cell lines. Compounds **1**, **3**, **7**, **10** and **11** were inactive to weakly active compounds against all of the tested cell lines. In addition, compounds **4**, **5**, **6** and **12** displayed cytotoxic activity against HuCCA-1 and MOLT-3 cell lines with lower IC_{50} values as compared to HepG2 and A549 cell lines.

The results demonstrated that substitution of the 2-Cl group of compound **1** with various amino groups afforded compounds with active and inactive cytotoxic activity. Substitution with alkylamino (**3**) and phenylalkylamino (**10** and **11**) substituents contributed to reduced cytotoxic activity while quinolinylamino (**5**) and phenylamino (**6**, **8** and **9**) substituents led to improved cytotoxic activity as compared to that of the 2,3-dichloroquinone compound (**1**). However, these active compounds were found to be less potent than that of the reference drug (doxorubicin) as deduced by IC_{50} values. It was noted that compounds **5**, **6**, **8** and **9** exhibited better cytotoxic activity against HepG2 cell than the reference drug, etoposide. Significantly improved cytotoxic activities were found in compounds bearing acetylphenylamino substituents (**8** and **9**). The enhanced effect of amino substituents is the following order: acetylphenylamino > quinolinylamino > alkylamino > phenylalkylamino.

Cytotoxicity of compounds **1** and **3–12** (Table 1) toward normal cell (MRC-5) revealed that quinones **3**, **10** and **11** were shown to be non-cytotoxic. Selectivity index (SI) of these compounds represented by the ratio of cytotoxicities between normal cell and different cancer cell lines is summarized in Table 2.

The results revealed that the most active cytotoxic compounds (**8** and **9**), particularly, compound **8** had higher SI on HepG2, HuCCA-1, and A549 with the respective values of 3.26, 6.58 and 1.26 as compared to compound **9** (SI = 1.26, 3.73 and 0.62, respectively). Inversely, compound **9** had higher SI value (5.79) on MOLT-3 as



- 3 : R = H, R' = *n*-C₄H₉
 4 : R = H, R' = C₆H₅
 5 : R = H, R' = 8-aminoquinolinyl
 6 : R = CH₃, R' = C₆H₅
 7 : R = H, R' = C₆H₄-CO₂H-*o*
 8 : R = H, R' = C₆H₄-COCH₃-*m*
 9 : R = H, R' = C₆H₄-COCH₃-*p*
 10 : R = H, R' = CH₂CH₂-C₆H₅
 11 : R = H, R' = CH₂CH₂-C₆H₃-3,4-diOMe
 12 : R = H, R' = C₆H₄-NH-C₆H₅-*p*

Scheme 1. Synthesis of aminonaphthoquinones derivatives 3–12 by nucleophilic substitution reaction of 2,3-dichloronaphthoquinone (1).

compared to compound **8** (SI = 4.87). It should be noted that compound **8** showed the highest SI value (6.58) on HuCCA-1 while the highest SI (5.79) of compound **9** was observed on MOLT-3 cell. Interestingly, the highest SI (11.46) among the investigated compounds was found to be compound **7** toward MOLT-3 cell.

Cytotoxic activities of the investigated 1,4-quinone analogs (**1** and **3–12**) against HepG2, HuCCA-1, A549, MOLT-3 and MRC-5 cells have not been previously reported before. So far, *N*-phenylamino (**4**) and *N*-methyl-*N*-phenylamino (**6**) 1,4-quinone analogs showed inhibitory effects against cancer cell lines (MCF-7, DU145 and T24) [25] whereas 2,3-dichloroquinone (**1**) displayed antiproliferative effect on cervical cancer (Hela) cells [5].

Cytotoxic effect of 1,4-quinone derivatives acts mainly by inhibiting the DNA topoisomerase II enzyme [38]. Furthermore, the quinone moiety can also produce ROS that causes DNA damage thereby leading to cell death [39,40]. Moreover, cytotoxic activity could also be explained by the electron accepting capability of compounds [24] in which the electrophilic center is prone to be attacked by cellular nucleophiles. On the basis of these principles, highly potent cytotoxic compounds are likely to require important molecular properties such as lipophilicity in reaching intracellular target sites, appropriate size, conformation or geometry for interacting with enzyme binding sites as well as good electron accepting capability to serve as target sites for cancer cells.

It can be deduced from the experimental results that the electron accepting capability of the 1,4-quinone compound is increased when one chlorine atom of the parent compound (**1**) was substituted with the phenylamino group as observed in compounds **6**, **8** and **9**, and with the quinolinylamino group as in compound **5**. Apparently, such substitutions enhanced the electrophilicity of the 1,4-quinone moiety in interacting with cellular nucleophiles by delocalizing nitrogen lone pair electrons to the phenyl ring which is directly connected to the amino group. In strike contrast, substitutions with alkylamino (**3**) and phenylalkylamino (**10** and **11**) groups afforded compounds with decreased cytotoxic activity as well as with non-cytotoxicity toward normal cell. This may be attributed to the fact that electron-donating effects of the alkyl group on the N-atom of amino groups could deactivate the reactivity of 1,4-quinone toward cellular nucleophilic attack.

2.3. QSAR study of cytotoxic activity

Quantum chemical and molecular descriptors of the 35 compounds (**1** and **3–36**) were calculated using Gaussian [41] and

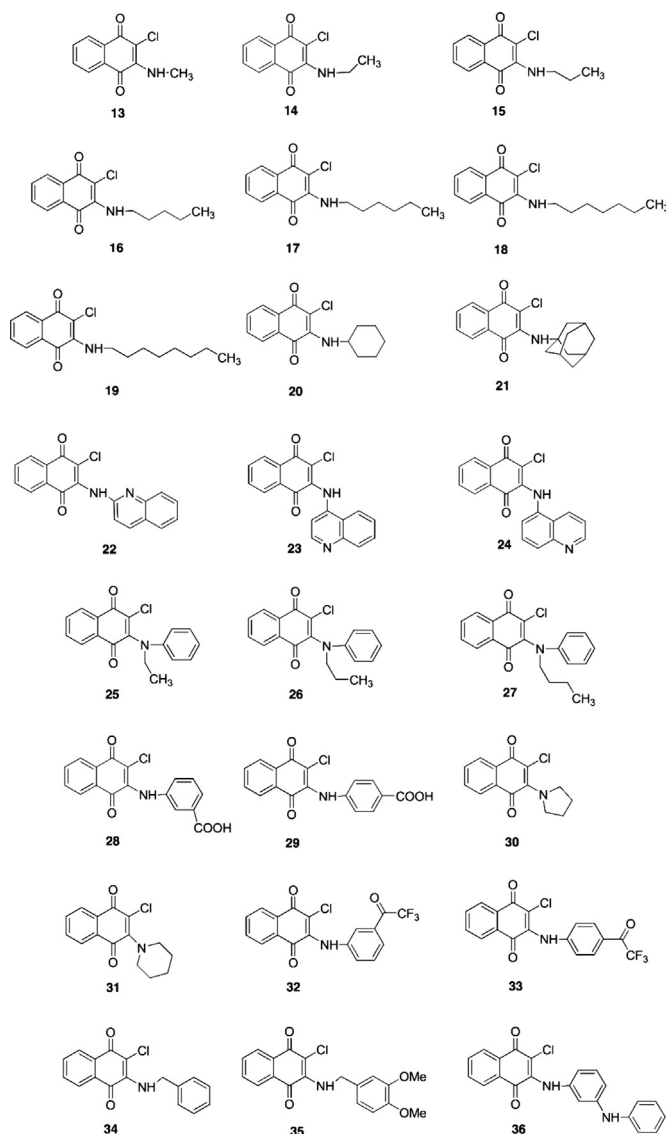


Fig. 2. Chemical structures of compounds 13–36.

Table 1
Cytotoxic activity of compounds **1** and **3–12** against four cancer cell lines and normal cell (MRC-5).

Compound	IC ₅₀ (μM)				MRC-5
	HepG2	HuCCA-1	A549	MOLT-3	
1	65.187 ± 4.38 ^a	19.204 ± 0.51 ^a	45.366 ± 0.56 ^a	13.037 ± 0.50 ^a	22.99 ± 0.42
3	64.462 ± 1.73 ^a	61.163 ± 4.20 ^a	81.829 ± 1.87 ^a	46.337 ± 2.30 ^a	non-cytotoxic
4	88.118 ± 5.00 ^a	8.636 ± 0.35 ^b	63.798 ± 5.83 ^a	3.489 ± 0.08 ^b	16.39 ± 1.28
5	12.935 ± 1.15 ^a	7.916 ± 0.64 ^b	53.769 ± 12 ^a	3.824 ± 0.34 ^b	13.59 ± 1.33
6	12.528 ± 0.55 ^a	5.206 ± 0.07 ^b	36.945 ± 5.66 ^a	3.157 ± 0.16 ^b	8.60 ± 0.77
7	81.38 ± 2.89 ^a	50.134 ± 0.66 ^a	inactive ^c	7.506 ± 1.07 ^b	86.05 ± 3.04
8	4.758 ± 0.78 ^b	2.364 ± 0.53 ^b	12.279 ± 1.41 ^a	3.193 ± 0.28 ^b	15.53 ± 0.75
9	9.731 ± 0.29 ^b	3.285 ± 1.03 ^b	19.647 ± 1.98 ^a	2.118 ± 0.03 ^b	12.28 ± 1.08
10	inactive ^c	inactive ^c	inactive ^c	29.061 ± 0.91 ^a	non-cytotoxic
11	71.730 ± 7.64 ^a	inactive ^c	inactive ^c	inactive ^c	non-cytotoxic
12	inactive ^c	10.672 ± 0.42 ^a	inactive ^c	9.178 ± 0.25 ^b	20.78 ± 0.68
Etoposide	20.389 ± 0.00	— ^d	— ^d	0.051 ± 0.01	— ^d
Doxorubicin	0.570 ± 0.13	0.239 ± 0.02	0.258 ± 0.03	— ^d	non-cytotoxic

^a Weakly active compound.^b Moderately active compound.^c Inactive compound.^d Not tested.

Dragon [42] to obtain 13 and 3224 descriptors, respectively. Redundant and highly correlated descriptors were removed using an in-house developed Monte Carlo–Multiple Linear Regression (MC–MLR) method or correlation-based. The remaining set of 10 significant descriptors was comprised of Mor04m, RDF050m, RDF060m, RDF065m, EEig03d, ESpm13d, R8v+, R5m, HATS4p and De. Definitions of these descriptors and the calculated values of significant descriptors are shown in Tables 3 and 4, respectively.

2.4. Evaluation of predictive performance of QSAR models

Details of the predictive performance of constructed QSAR models are shown in Table 5 in which the HuCCA-1 model provided the best performance as observed from R_{CV} and $RMSE_{CV}$ values of 0.9753 and 0.1146, respectively. Experimental and predicted pIC_{50} values of cytotoxic activity of compounds **1** and **3–12** as tested against four cancer cell lines are summarized in Table 6 and Fig. 3.

2.5. Prediction of structurally modified compounds (**13–36**) using QSAR models

Predicted pIC_{50} values of 24 modified compounds **13–36** (Fig. 2) were calculated according to the QSAR equations (Table 5) as a function of significant descriptor values (Table 4). Compounds **13–36** were categorized by their predicted cytotoxic activities as highly active ($pIC_{50} > 0$), moderately active ($-1 < pIC_{50} < 0$) and weakly active to inactive ($pIC_{50} < -1$) [37]. The predicted pIC_{50}

Table 2
Selectivity index (SI) of compounds **1** and **3–12**.

Compound	SI ^a			
	HepG2	HuCCA-1	A549	MOLT-3
1	0.35	1.20	0.51	1.76
3	ND	ND	ND	ND
4	0.19	1.90	0.26	4.70
5	1.05	1.72	0.25	3.56
6	0.69	1.65	0.23	2.72
7	1.06	1.72	ND	11.46
8	3.26	6.58	1.26	4.87
9	1.26	3.73	0.62	5.79
10	ND	ND	ND	ND
11	ND	ND	ND	ND
12	ND	1.95	ND	2.26

^a SI = IC_{50} normal cell/ IC_{50} cancer cell. ND = not determine.

values of structurally modified compounds (**13–36**) against the four tested cell lines are shown in Table 7.

2.6. QSAR analysis and molecular descriptor interpretations

QSAR modeling utilizing the MLR method had successfully been demonstrated on a wide range of chemical and biological properties [33–35]. Therefore, experimental IC_{50} values of eleven tested compounds (**1** and **3–12**) were employed for constructing QSAR models against four data sets corresponding to the four tested cell lines i.e. HepG2, HuCCA-1, A549 and MOLT-3. For each data set, compounds with inactive cytotoxic activity were excluded from the analysis. In order to improve the statistical quality of the model, outlying compounds were identified using Eq. (2) as described in the experimental section. Herein, compound **4** was identified as an outlier for the HuCCA-1 model and was subjected to removal whereas none of the outliers were identified in HepG2, A549 and MOLT-3 models.

Interpretation of molecular descriptors was performed by analyzing the relationship between the identified significant descriptors and their respective pIC_{50} values obtained by two data

Table 3
Definition of descriptors using for development of QSAR models.

Descriptor	Type	Definition
Mor04m	3D-MorSE descriptors	3D-MorSE–signal 04/weighted by atomic masses
RDF050m	RDF descriptors	Radial distribution function-5.0/weighted by atomic masses
RDF060m	RDF descriptors	Radial distribution function-6.0/weighted by atomic masses
RDF065m	RDF descriptors	Radial distribution function-6.5/weighted by atomic masses
EEig03d	Edge adjacency indices	Eigenvalue 03 from edge adjacency matrix weighted by dipole moments
ESpm13d	Edge adjacency indices	Spectral moment 13 from edge adjacency matrix weighted by dipole moments
R8v+	GETAWAY descriptors	R maximal autocorrelation of lag 8/ weighted by van der Waals volume
R5m	GETAWAY descriptors	R autocorrelation of lag 5/weighted by atomic masses
HATS4p	GETAWAY descriptors	Leverage-weighted autocorrelation of lag 4/ weighted by atomic polarizabilities
De	WHIM descriptors	D total accessibility index/weighted by Sanderson electronegativities

Table 4
Values of significant molecular descriptors for predicting the cytotoxic activity of four cell lines.

Compound	Mor04m	R8v+	RDF065m	RDF050m	RDF060m	EEig03d	ESpm13d	R5m	HATS4p	De
1	1.23	0	5.89	8.77	5.842	2.82	17.829	0.427	0.194	0.380
3	0.819	0.008	4.217	8.205	5.049	2.734	17.699	0.348	0.143	0.404
4	0.611	0.012	7.003	13.899	8.1	2.805	17.712	0.653	0.202	0.476
5	0.861	0.026	8.381	20.974	7.182	3.079	17.752	0.625	0.208	0.447
6	1.103	0.015	11.549	11.461	9.176	3.061	17.827	0.647	0.205	0.491
7	0.248	0.012	7.334	16.143	12.538	3.398	18.018	0.685	0.185	0.505
8	1.634	0.024	9.284	18.243	12.134	3.399	17.964	0.623	0.193	0.500
9	1.108	0.02	11.011	15.136	8.449	3.399	17.961	0.593	0.205	0.512
10	0.441	0.016	5.763	7.867	7.332	2.761	17.708	0.339	0.170	0.385
11	0.095	0.01	7.633	10.577	9.135	3.208	17.779	0.393	0.144	0.491
12	0.708	0.008	9.37	15.387	11.233	2.885	17.73	0.554	0.165	0.490
13	0.492	0.008	3.786	6.317	2.937	2.725	17.695	0.400	0.164	0.369
14	0.908	0.009	3.787	6.551	3.647	2.732	17.698	0.446	0.125	0.383
15	0.51	0.008	4.245	7.008	5.091	2.733	17.699	0.394	0.140	0.391
16	0.598	0.012	4.431	8.564	5.082	2.734	17.699	0.321	0.14	0.410
17	0.513	0.01	5.291	8.796	5.055	2.734	17.699	0.305	0.134	0.420
18	0.563	0.008	6.251	9.095	5.236	2.734	17.699	0.321	0.135	0.425
19	0.251	0.006	7.18	9.197	5.113	2.734	17.699	0.290	0.125	0.433
20	0.144	0.009	7.187	7.526	9.394	2.805	17.712	0.499	0.169	0.442
21	-0.134	0.008	7.822	12.114	10.71	3.383	17.967	0.480	0.185	0.435
22	0.818	0.028	11.963	16.037	9.194	2.958	17.733	0.619	0.216	0.474
23	0.336	0.024	9.203	16.047	8.056	3.079	17.752	0.619	0.205	0.465
24	1.47	0.018	8.325	22.359	8.878	3.079	17.752	0.587	0.187	0.525
25	1.179	0.013	10.123	11.192	9.031	3.097	17.844	0.689	0.149	0.488
26	0.833	0.013	11.354	13.387	9.664	3.102	17.846	0.693	0.143	0.421
27	0.75	0.012	11.804	14.038	8.27	3.102	17.846	0.651	0.145	0.382
28	1.273	0.014	8.969	17.264	9.72	3.399	17.991	0.612	0.182	0.505
29	1.016	0.023	13.419	14.337	8.44	3.399	17.988	0.642	0.216	0.522
30	1.909	0.011	6.348	11.652	4.969	2.963	17.801	0.654	0.203	0.431
31	1.387	0.01	7.417	10.857	5.705	2.955	17.799	0.601	0.199	0.430
32	2.486	0.024	10.87	18.273	16.471	3.399	19.888	0.780	0.188	0.513
33	1.353	0.02	12.992	14.278	8.729	3.399	19.888	0.732	0.199	0.536
34	1.04	0.014	5.17	7.626	5.172	2.81	17.711	0.380	0.174	0.394
35	0.764	0.01	7.758	12.165	6.101	3.21	17.782	0.471	0.155	0.475
36	0.871	0.011	9.329	15.627	9.658	2.914	17.731	0.533	0.137	0.438

sets comprising of tested compounds (**1** and **3–12**) and virtually constructed compounds (**13–36**). As to afford a more uniform distribution of data values, IC_{50} were converted to pIC_{50} by taking the negative logarithm to the base of 10. Therefore, high pIC_{50} values represented low IC_{50} values indicating potent cytotoxic activity whereas low pIC_{50} values represented high IC_{50} value indicating less potent activity.

2.6.1. HepG2 and HuCCA-1 models

Similar results were found in both HepG2 and HuCCA-1 models in which important descriptors concerning atomic masses were governing the cytotoxic activity. The most potent compound against each cell line is represented as the highest pIC_{50} values. In both models, the highest cytotoxic activity among those investigated was compound **8** while that of the virtual constructs was observed in compound **32**.

The QSAR equation of the HepG2 model is shown below:

$$pIC_{50} = 0.5509(\text{Mor04m}) + 38.3151(\text{R8v+}) - 2.4803$$

R8v+ representing the van der Waals volume seems to be the most important descriptor as deduced from its highest regression coefficient value of 38.3151. The highest R8v+ (0.024) and high Mor04m (1.634) values among the tested compounds were both found in compound **8** (Table 4). Compound **32** (a trifluoroacetyl analog of compound **8**) exhibited the most potent predicted cytotoxic activity among the series of modified compounds as shown in Table 7. Particularly, structural modification of compound **8** by replacing the hydrogen atom of acetyl group with a fluorine atom bearing higher atomic number to obtain compound **32** could significantly improve the Mor04m (2.486) value by 1.52 folds as compared to its parent compound **8** (Mor04m = 1.634). The results showed that the predicted pIC_{50} values of compound **8** (Table 6)

Table 5
Summary of QSAR equations and their predictive performances in predicting cytotoxic activity of naphthoquinone derivatives against four cell lines.

Cell line	Equation	N	R_{Tr}	RMSE _{Tr}	R_{CV}	RMSE _{CV}
HepG2	$pIC_{50} = 0.5509(\text{Mor04m}) + 38.3151(\text{R8v+}) - 2.4803$	9	0.9532	0.1400	0.9177	0.1881
HuCCA-1	$pIC_{50} = 0.1159(\text{RDF065m}) + 0.739(\text{Mor04m}) + 0.029(\text{RDF050m}) - 3.1356$	8	0.9941	0.0526	0.9753	0.1146
A549	$pIC_{50} = 0.0386(\text{RDF060m}) + 0.0599(\text{EEig03d}) + 1.8865(\text{ESpm13d}) - 35.6888$	7	0.9952	0.0266	0.9745	0.0614
MOLT-3	$pIC_{50} = -0.699(\text{R5m}) + 15.5389(\text{HATS4p}) + 5.6347(\text{De}) - 5.9617$	10	0.9860	0.0708	0.9624	0.1187

pIC_{50} is the concentration of compound required for 50% inhibition of cell growth.

N is a number of data set.

R_{Tr} is a correlation coefficient of the training set.

RMSE_{Tr} is a root mean square error of the training set.

R_{CV} is a correlation coefficient of leave-one-out cross validation (LOO-CV) of the testing set.

RMSE_{CV} is a root mean square error LOO-CV of the testing set.

Table 6
Experimental and predicted cytotoxic activities (pIC₅₀) of compounds **1** and **3–12** against four cancer cell lines.

Compound	HepG2		HuCCA-1		A549		MOLT-3	
	Exp.	Pred.	Exp.	Pred.	Exp.	Pred.	Exp.	Pred.
1	-1.814	-1.775	-1.283	-1.217	-1.657	-1.669	-1.115	-1.094
3	-1.809	-1.703	-1.786	-1.597	-1.913	-1.961	-1.666	-1.762
4	-1.945	-1.64	outlier	outlier	-1.805	-1.783	-0.543	-0.614
5	-1.112	-0.942	-0.899	-0.802	-1.731	-1.751	-0.583	-0.688
6	-1.098	-1.332	-0.717	-0.523	-1.568	-1.506	-0.499	-0.453
7	-1.911	-1.872	-1.700	-1.286	- ^a	- ^a	-0.875	-0.608
8	-0.677	-0.643	-0.374	-0.305	-1.089	-1.214	-0.504	-0.598
9	-0.988	-1.13	-0.517	-0.619	-1.293	-1.232	-0.326	-0.247
10	- ^a	-1.463	-1.333					
11	-1.856	-2.182	- ^a					
12	- ^a	- ^a	-1.028	-1.001	- ^a	- ^a	-0.963	-1.059

^a – = the compound was experimentally inactive and was excluded from the data set of QSAR analysis.

and compound **32** (Table 7) towards HepG2 were -0.643 and -0.191, respectively. This led to marked improvements (3.39 folds) in the cytotoxic activity of compound **32** when compared to compound **8** as represented by the higher pIC₅₀ value of the analog **32**.

The worst predicted cytotoxic activity against HepG2 cell line was found in compound **21** in which the negative Mor04m value of -0.134 (Table 4) was found in concomitant with low pIC₅₀ value of -2.248 (Table 7). Chemical structure of compound **21** was modified from compound **4** by replacing the phenylamino moiety with the 1-adamantyl amino group. The loss of cytotoxic activity is plausibly due to steric hindrance of the bulky 1-adamantyl group that affects its binding to the active site of DNA topoisomerase II.

The QSAR equation of the HuCCA-1 model is shown below:

$$\text{pIC}_{50} = 0.1159(\text{RDF065m}) + 0.739(\text{Mor04m}) + 0.029(\text{RDF050m}) - 3.1356$$

It can be seen that the Mor04m descriptor is primarily responsible for prediction of the cytotoxic activity of HuCCA-1 cell line as deduced from its high regression coefficient value of 0.739. Similarly, the trifluoroacetyl analog **32** (Mor04m = 2.486) could significantly increase the value of the atomic mass descriptor Mor04m by 1.52 folds when compared to the acetyl compound **8** (Mor04m = 1.634) thereby leading to markedly improved cytotoxic activity. However, the cytotoxic activity of compound **32** (pIC₅₀ = 0.491) against HuCCA-1 was 1.26 folds less potent than the reference drug, doxorubicin, showing pIC₅₀ value of 0.621 (Table 7). On the other hand, the worst predicted cytotoxic activity against HuCCA-1 cell line (Table 7) was found to be compound **13** (pIC₅₀ = -2.150) which also had the lowest atomic masses weighted descriptor values of 3.786 for RDF065m and 6.317 for RDF050m as shown in Table 4. It could be explained that compound **13** has the methylamino group on the 1,4-quinone core structure in which methyl is the smallest group on the amino moiety among the investigated series.

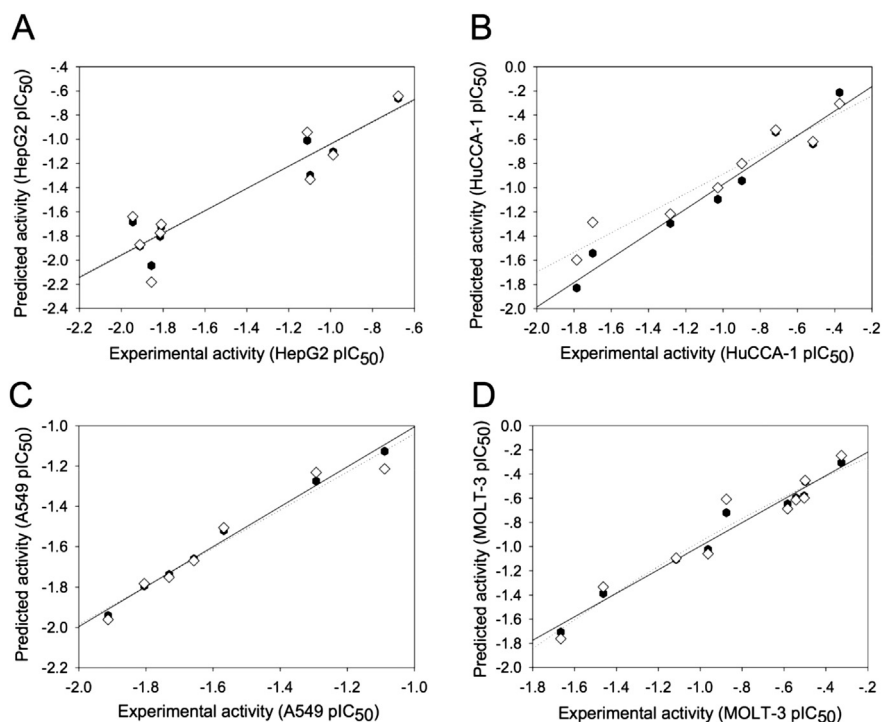


Fig. 3. Plots of experimental versus predicted pIC₅₀ values of cytotoxic activities against four cell lines (A: HepG2, B: HuCCA-1, C: A549, D: MOLT-3) generated by QSAR models (training set: compounds are represented by closed hex and regression line is shown as a solid line, leave-one-out validated testing set: compounds are represented by open diamond and regression line is shown as a dotted line).

Table 7
Predicted cytotoxic activity (pIC₅₀) of modified compounds (**13–36**) and experimental cytotoxic activity of reference drugs.

Compound	pIC ₅₀			
	HepG2	HuCCA-1	A549	MOLT-3
13	-1.903 ^a	-2.150 ^a	-2.031 ^a	-1.614 ^a
14	-1.635 ^a	-1.836 ^a	-1.997 ^a	-2.173 ^a
15	-1.893 ^a	-2.063 ^a	-1.939 ^a	-1.858 ^a
16	-1.691 ^a	-1.932 ^a	-1.940 ^a	-1.700 ^a
17	-1.815 ^a	-1.888 ^a	-1.941 ^a	-1.726 ^a
18	-1.864 ^a	-1.731 ^a	-1.934 ^a	-1.694 ^a
19	-2.112 ^a	-1.851 ^a	-1.939 ^a	-1.782 ^a
20	-2.056 ^a	-1.978 ^a	-1.744 ^a	-1.194 ^a
21	-2.248 ^a	-1.977 ^a	-1.178 ^a	-0.971 ^b
22	-0.957 ^b	-0.680 ^b	-1.703 ^a	-0.367 ^b
23	-1.376 ^a	-1.355 ^a	-1.704 ^a	-0.589 ^b
24	-0.981 ^b	-0.436 ^b	-1.673 ^a	-0.508 ^b
25	-1.333 ^a	-0.767 ^b	-1.492 ^a	-1.378 ^a
26	-1.523 ^a	-0.816 ^b	-1.463 ^a	-1.852 ^a
27	-1.607 ^a	-0.806 ^b	-1.517 ^a	-2.011 ^a
28	-1.243 ^a	-0.655 ^b	-1.170 ^a	-0.716 ^{b,c}
29	-1.039 ^a	-0.414 ^b	-1.225 ^a	-0.113 ^{b,c}
30	-1.007 ^a	-0.651 ^b	-1.738 ^a	-0.836 ^b
31	-1.333 ^a	-0.936 ^b	-1.714 ^a	-0.867 ^b
32	-0.191 ^{b,c}	0.491 ^{c,d}	2.669 ^{c,d,e}	-0.695 ^b
33	-0.969 ^b	-0.216 ^b	2.370 ^{d,e}	-0.361 ^b
34	-1.371 ^a	-1.545 ^a	-1.909 ^a	-1.303 ^a
35	-1.676 ^a	-1.319 ^a	-1.715 ^a	-1.206 ^a
36	-1.579 ^a	-0.958 ^b	-1.692 ^a	-1.737 ^a
Etoposide ^f	-1.309	-g	-g	1.292
Doxorubicin ^f	0.244	0.621	0.588	-g

^a Weakly active to inactive compound.

^b Moderately active compound.

^c The most potent compound against each cancer cell line.

^d Highly active compound.

^e Compound with more potent cytotoxic activity compared to reference drugs.

^f Experimental pIC₅₀ values.

^g Not tested.

2.6.2. A549 model

Besides atomic masses, dipole moment properties of compounds are highly involved in cytotoxic activity against the A549 cell line as shown by the QSAR equation below:

$$\text{pIC}_{50} = 0.0386(\text{RDF060m}) + 0.0599(\text{EEig03d}) \\ + 1.8865(\text{ESpm13d}) - 35.6888$$

It is noted that high regression coefficients were observed for dipole moment weighted descriptors, particularly ESpm13d, which is shown to be more important in predicting the cytotoxic activity as compared to atomic mass weighted descriptor, RDF060m.

Interestingly, isomeric trifluoroacetyl compounds **32** (pIC₅₀ = 2.669) and **33** (pIC₅₀ = 2.370), which are derivatives of the corresponding acetyl compounds **8** and **9**, exhibited significantly more potent cytotoxic effect against A549 cell line when compared to doxorubicin (pIC₅₀ = 0.588). This indicated that the respective pIC₅₀ values of *m*- (**32**) and *p*- (**33**) compounds were approximately 4.5 folds and 4 folds higher than that of the reference drug. These results showed that the fluorine atom may improve the lipophilicity of such compounds thereby allowing them to reach intracellular target sites. As shown in Table 4, both compounds (**32** and **33**) possessed exactly the same values for dipole moment weighted descriptors, EEig03d (3.399) and ESpm13d (19.888), while bearing different values for the atomic mass weighted descriptor, RDF060m (16.471 and 8.729, respectively). Moreover, compound **32** had RDF060m value of 2 folds greater than that of compound **33**. Such high RDF060m value of compound **32** could plausibly be attributed to the effect of substituent on the *m*-position that makes the compound with more appropriate shape in

interacting with the target site as compared to *p*-compound **33**. Similar findings were found for *m*-acetyl compound **8** in which its higher RDF060m value (12.134) afforded better cytotoxic activity when compared to *p*-acetyl compound **9** with RDF060m value of 8.449. Apparently, compounds with *m*-acetylphenylamino (**8**) or *m*-trifluoroacetylphenylamino (**32**) substituents exhibited more potent cytotoxic activity than the corresponding *para*-substituents (**9** and **33**). Similar effects of *m*- and *p*-acetyl substituents on the phenyl ring (**8**, **9**, **32** and **33**) were noted for the prediction of cytotoxic activity against HepG2 and HuCCA-1 cell lines.

It could be assumed from these findings that the *ortho*, *meta* and *para* position of substituents could affect the cytotoxic activity in which only particular isomers can act as potent anticancer agents.

2.6.3. MOLT-3 model

Distinct from other cell lines, the cytotoxic activity of compounds against the MOLT-3 cell line is dependent on atomic polarizability, electronegativity and atomic mass as shown in the equation below:

$$\text{pIC}_{50} = -0.699(\text{R5m}) + 15.5389(\text{HATS4p}) + 5.6347(\text{De}) \\ - 5.9617$$

It can be noted that the atomic polarizability-weighted descriptor (HATS4p) was the most influential descriptor for predicting the cytotoxic activity owing to the fact that it afforded the highest regression coefficient value (15.5389). The electronegativity-weighted descriptor (De) ranked the second most important one affording regression coefficient of 5.6347 while atomic mass-weighted descriptor (R5m) plays its minimal role with negative regression coefficient of -0.699. According to the QSAR equation, high HATS4p and high De values together with low R5m value are likely required for potent cytotoxic activity. It was found that *p*-amino benzoic acid analog **29** was predicted as the most potent anticancer agent against MOLT-3 cell line as represented by the highest predicted pIC₅₀ value of -0.113 (Table 7). However, such compound exhibited approximately 11.4 folds less potent activity than the reference drug, etoposide (pIC₅₀ = 1.292, Table 7). The potent cytotoxic activity of compound **29** could possibly be governed by its high HATS4p and De values resulting from high electronegativity O-atom of CO₂H group that can be polarized and withdraw lone pair electron on N-atom of amino group, giving rise to a significantly improved redox potential of the compound. Within the same series of isomeric amino benzoic acid analogs (**7**, **28** and **29**), the *p*-amino benzoic acid analog (**29**) provided the highest HATS4p value (0.216, Table 4) as compared to *ortho* (**7**) and *meta* (**28**) analogs with HATS4p values of 0.185 and 0.182, respectively (Table 4). The analog **29** had approximately 5 and 6 folds greater activity than *ortho* (**7**) and *meta* (**28**) analogs in which their predicted pIC₅₀ values were -0.608 (Table 6) and -0.716 (Table 7), respectively. In addition, isomeric effects of COCH₃ group at *m*- and *p*-positions can significantly affect polarizability of the compounds by decreasing HATS4p values from *p*- to *m*-analogs as found in compounds **9** and **8** with the values of 0.205 and 0.193, respectively (Table 4). In case of COCF₃ analogs **32** and **33**, their HATS4p values were decreased as compared to acetyl analogs **8** and **9**, and shown to be 0.188 and 0.199, respectively. Apparently, the reduced polarizabilities values of **32** and **33** could be due to the lipophilic effect of trifluoroacetyl group. These results revealed that substitution of acetyl (**9**), trifluoroacetyl (**33**) and carboxyl (**29**) groups at *para* position on phenylamino moiety enhances cytotoxic activity of compounds against MOLT-3 cell line while substitution at *meta* and *ortho* positions aggravates the activity. In contrast, substitution of these functional groups at *meta* position seems to be the

appropriate strategy for developing anticancer agents against HepG2, HuCCA-1 and A549 cell lines.

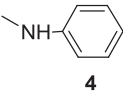
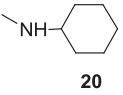
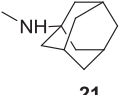
Previously, QSAR study of antiproliferative and cytotoxic activities of 1,4-naphthoquinone derivatives against the L1210 cell line demonstrated that the hydrophobic effect is an important parameter for defining the bioactivities [43]. Herein, the trifluoroacetyl compound **33** exhibited the second most potent activity against MOLT-3 cell line among all of structural modified compounds affording the predicted pIC_{50} value of -0.361 (Table 7). However, compound **33** is less potent than its parent compound (**9**). This could be due to the fact that replacement of acetyl group in compounds **8** and **9** with trifluoroacetyl group can significantly increase atomic mass-weighted descriptor ($R5m$) value leading to higher lipophilicity (or lower polarizabilities) that decreased cytotoxic activity as demonstrated in compounds **32** and **33**. The $R5m$ values of compounds **8**, **9**, **32** and **33** are 0.623, 0.593, 0.780 and 0.732, respectively (Table 4). Such results indicate HAPS4p as the most influential descriptor governing the cytotoxic activity toward MOLT-3 cell line. Interestingly, these findings are different from those of HepG2, HuCCA-1 and A549 cell lines in which fluorine analogs (**32** and **33**) exhibited more potent activity as compared to their parents compounds (**8** and **9**) by improving lipophilicity of the compounds thereby enhancing cell entry to reach their target sites.

Regarding the effect of fluorine substitution deteriorating cytotoxic activity against MOLT-3 cell line by increasing atomic mass-weight descriptor value ($R5m$), it could be hypothesized that besides the lipophilicity, the appropriate atomic polarizabilities and masses or size of the molecules are crucial for exerting potent cytotoxic activity against MOLT-3 cell line in terms of cell entry and interaction at intracellular target sites.

The effect of modifications to chemical structures on descriptor values and cytotoxic activity against the four investigated human cancer cell lines are summarized in Tables 8–11. Particularly, the experimental pIC_{50} of tested compounds **1** and **3–12** and the predicted pIC_{50} of virtual constructs **13–36** along with their significant descriptor values were provided. It can be deduced that substituents (R) on the 2-amino position of 1,4-naphthoquinone core structures (Figs. 1 and 2) may affect the cytotoxic activity of compounds by improving or aggravating it, which depends on molecular properties of compounds that are influenced by their substituents. Apparently, compounds which R = acetylphenyl groups (**8** and **9**) were found to be the most potent anticancer agents. Moreover, fluorine substituents (R = trifluoroacetylphenyl) of virtually constructed compounds (**32** and **33**) exhibited markedly improved cytotoxic activity against every cancer cell lines except for MOLT-3 cell. Furthermore, some particular isomers seemed to

Table 8

The effect of phenyl and cycloalkane rings on values of significant descriptors and cytotoxic activity against four cell lines.

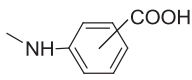
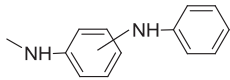
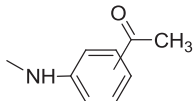
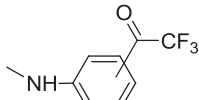
Effect of substituent	HepG2	HuCCA-1	A549	MOLT-3
Most potent compound	32	32	32^a	29
Worst potent compound	21	13	13	14
	↓ Mor04m ^b ↓ activity ^b	↓ Mor04m ^b ↑ RDF065m ^b ↑ RDF050m ^b ↑ activity ^b	↓ ESpm13d ^b ↓ activity ^b	↑ all descriptors ^b ↑ activity ^b
	↓ Mor04m ^b ↓ activity ^b	↓ Mor04m ^b ↓ activity ^b	↓ ESpm13d ^b ↓ activity ^b	↓ HATS4p ^b ↑ R5m ^b ↓ activity ^b
	↓ Mor04m ^b ↓ activity ^b	↓ Mor04m ^b ↓ activity ^b	↑ all descriptors ^b ↑ activity ^b	↓ HATS4p ^b ↑ R5m ^b ↑ De ^b ↑ activity ^b
	↑ Mor04m ^b ↑ activity ^b	↑ Mor04m ^b ↑ activity ^b	↓ ESpm13d ^b ↓ activity ^b	↑ all descriptors ^b ↑ activity ^b
	↑ Mor04m ^b ↑ activity ^b	↑ Mor04m ^b ↑ activity ^b	↓ ESpm13d ^b ↓ activity ^b	↑ R5m ^b ↑ De ^b ↑ activity ^b
Fluorine substituents (32 & 33)	↑ all descriptors ^b ↑ activity ^b	↑ all descriptors ^b ↑ activity ^b	↑ ESpm13d ^b ↑ RDF060m ^b ↑ activity ^b	↑ R5m ^b ↑ De ^b ↑ activity ^b

^a More potent than reference drug, doxorubicin.

^b Comparison of descriptor values and cytotoxic activity of considered compound and compound **1**.

Table 9

The effect of substituted phenyl on values of significant descriptors and cytotoxic activity against four cell lines.

Effect of substituent	HepG2	HuCCA-1	A549	MOLT-3
 7: ortho 28: meta 29: para	Mor04m ^a : 28 > 29 > 7 activity ^a : 29 > 28 > 7 activity ^b : 7↓, 28↑, 29↑ para > meta > ortho	Mor04m ^a : 28 > 29 > 7 activity ^a : 29 > 28 > 7 activity ^b : 7↓, 28↑, 29↑ para > meta > ortho	ESpm13d ^a : 28 > 29 > 7 activity ^a : 28 > 29 > 7 activity ^b : 7↓, 28↑, 29↑ meta > para > ortho	HATS4p ^a : 29 > 7 > 28 activity ^a : 29 > 7 > 28 activity ^b : 7↑, 28↑, 29↑↑ para > ortho > meta
 12: para 36: meta	Mor04m ^a : 36 > 12 R8v ^a : 36 > 12 activity ^a : 36 > 12 activity ^b : 12↓, 36↑ meta > para	Mor04m ^a : 36 > 12 RDF050m ^a : 36 > 12 activity ^a : 36 > 12 activity ^b : 12↑, 36↑ meta > para	EEig03d ^a : 36 > 12 RDF060m ^a : 12 > 36 activity ^a : 36 > 12 activity ^b : 12↓, 36↓ meta > para	HATS4p ^a : 12 > 36 De ^a : 12 > 36 activity ^a : 12 > 36 activity ^b : 12↑, 36↓ para > meta
 8: meta 9: para	Mor04m ^a : 8 > 9 activity ^a : 8 > 9 activity ^b : 8↑, 9↑ meta > para	Mor04m ^a : 8 > 9 activity ^a : 8 > 9 activity ^b : 8↑, 9↑ meta > para	RDF060m ^a : 8 > 9 activity ^a : 8 > 9 activity ^b : 8↑, 9↑ meta > para	HATS4p ^a : 9 > 8 R5m ^a : 8 > 9 activity ^a : 9 > 8 activity ^b : 8↑, 9↑ para > meta
 32: meta 33: para	Mor04m ^a : 32 > 33 activity ^a : 32 > 33 activity ^b : 32↑, 33↑ meta > para	Mor04m ^a : 32 > 33 activity ^a : 32 > 33 activity ^b : 32↑, 33↑ meta > para	RDF060m ^a : 32 > 33 activity ^a : 32^c > 33^c activity ^b : 32↑, 33↑ meta > para	HATS4p & De ^a : 33 > 32 R5m ^a : 32 > 33 activity ^a : 33 > 32 activity ^b : 32↑, 33↑ para >> meta

^a Comparison within the same series.^b Comparison of descriptor values and cytotoxic activity of considered compound and compound 1.^c More potent than reference drug, doxorubicin.

be more cytotoxic against particular cell lines as shown by the effects caused by variations of substituents at the *ortho*, *meta* and *para*-positions as well as length of alkyl chain and position of quinolonyl substituents.

2.7. Molecular descriptor interpretations based on mechanisms of action of the reference drugs

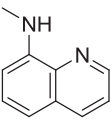
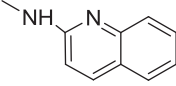
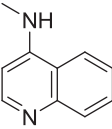
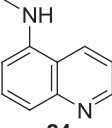
The steps of DNA unwinding is a crucial process for DNA synthesis whereby it allows the separation of complementary DNA strands to facilitate initiation and elongation processes of DNA replication [3]. The DNA unwinding process is catalyzed by the homodimeric enzyme known as topoisomerase II [3]. Topoisomerase II is the essential enzyme that regulates the DNA winding and unwinding processes. DNA topoisomerase II functions in a cyclic fashion [3] and ATP is required as a cofactor for driving the catalytic cycle as well as for enzyme recycling [44]. The catalytic cycle initiates when topoisomerase II binds double-stranded DNA to form the enzyme–DNA cleavage complex [29]. Topoisomerase II then cleaves one of the DNA strands creating a transient strand break thereby allowing the passage of another intact DNA region [29]. After the DNA passage is completed, the transient DNA strand break is religated and the enzyme is released from the cleavage complex [29] to be reused in further catalytic cycles [44]. Thus far, topoisomerase II is one of the promising targets for the treatment of cancers [3,30] owing to its potential to be genotoxic [3] as it creates transient DNA damage each time it functions [3]. An appropriate concentration of enzyme–DNA cleavage complex is essential for

normal cellular functions [45] and it can be altered by exogenous compounds such as anticancer drugs [3]. As the concentration of enzyme–DNA cleavage complex becomes too low, it gives rise to mitotic failure, slow cell growth and cell death [46–49]. Whereas when the concentration becomes too high, this induces the conversion of transient DNA breaks to permanent DNA damages [48] thereby leading to cell death [50]. In other words, the essential topoisomerase II enzyme is converted to cellular toxin known as topoisomerase poison [3]. The alteration of these steps in catalytic cycle can increase the concentration of enzyme–DNA cleavage complex. Such anticancer drugs exert their cytotoxic activity as topoisomerase poison by inhibiting religation of transient DNA-strand breaks thereby maintaining the enzyme–DNA cleavage complexes. As a result, the high level of enzyme–DNA cleavage complexes inhibits DNA synthesis subsequently leading to cell death [3,29,30].

Topoisomerase II poison can be classified by its mechanism of action as non-intercalative and intercalative types. Both mechanisms of action increase the concentration of enzyme–DNA cleavage complex resulting in cell death. However, non-intercalative type interacts at enzyme–DNA interfaces whereas the intercalative type intercalates DNA strands to cause structural changes of DNA [3].

Both reference drugs employed in this study are clinically used topoisomerase II poison. Therefore, their mechanism of actions could be reasonably applied for describing the structure–activity relationships through the utilization of identified significant descriptors and predicted cytotoxic activities.

Table 10
The effect of quinolinyl ring on values of significant descriptors and cytotoxic activity against four cell lines.

Effect of substituent	HepG2	HuCCA-1	A549	MOLT-3
Quinolinylamino position	activity ^a 5 > 22 > 24 > 23	activity ^a 24 > 22 > 5 > 23	activity ^a 24 > 22 ≈ 23 > 5	activity ^a 22 > 24 > 23 > 5
 5	↑R8v ⁺ , ↑activity ^b	↑RDF050m ^b ↑RDF065m ^b ↑activity ^b	↑EEig03d ^b ↓ESpm13d ^b ↓activity ^b	↑all descriptors ^b ↑activity ^b
 22	↑R8v ⁺ , ↑activity ^b	↑RDF050m ^b ↑RDF065m ^b ↑activity ^b	↓ESpm13d ^b ↓activity ^b	↑all descriptors ^b ↑activity ^b
 23	↑R8v ⁺ , ↑activity ^b	↑RDF050m ^b ↑RDF065m ^b ↓activity ^b	↓ESpm13d ^b ↓activity ^b	↑all descriptors ^b ↑activity ^b
 24	↑R8v ⁺ , ↑activity ^b	↑all descriptors ^b ↑activity ^b	↓ESpm13d ^b ↓activity ^b	↓HATS4p ^b ↑R5m ^b ↑De ^b ↑activity ^b

^a Comparison within the same series.

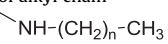
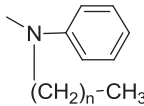
^b Comparison of descriptor values and cytotoxic activity of considered compound and compound 1.

Doxorubicin is an intercalative topoisomerase II poison containing the 1,4-quinone moiety as shown in Fig. 4. The cytotoxic effect of doxorubicin arises from its dual action as topoisomerase II catalytic inhibitor and topoisomerase II poison [3,29,30]. Firstly, doxorubicin acts as a topoisomerase inhibitor as to inhibit the topoisomerase II catalytic cycle. The planar structure of doxorubicin enhances its intercalation between DNA base pairs [29] giving rise to DNA structural changes [30] thereby prevents the binding of topoisomerase II with DNA strands in the initial step of the catalytic cycle [29] as well as creates permanent DNA damages [29]. Secondly, doxorubicin acts as a topoisomerase II poison by increasing and stabilizing enzyme–DNA cleavage complexes [29]. Moreover, the 1,4-quinone moiety of doxorubicin plays an important role in

the production of ROS leading to oxidative damages to the cells [30].

Etoposide (Fig. 4) is a non-intercalative topoisomerase II poison that acts by inhibiting the religation of transient DNA breaks [29,30]. Etoposide metabolites such as semiquinone and phenoxyl radical serve as ROS sources thereby leading to cellular damages [30]. Moreover, semiquinone metabolite is a potent inhibitor of the topoisomerase II–DNA cleavage complex [51,52] that directly binds to the DNA content of topoisomerase II–DNA cleavage complex [29] and finally resulting in the inhibition of DNA religation. As a consequence, the increasing level of topoisomerase II–DNA cleavage complex eventually causes cell death [3,29,30]. Such ROS including superoxide (O₂⁻) and hydroxyl radical (OH^{*}), which can

Table 11
The effect of hydrocarbon chain length on values of significant descriptors and cytotoxic activity against four cell lines.

Effect of substituent	HepG2	HuCCA-1	A549	MOLT-3
Length of alkyl chain  3,13,14,15,16,17,18 and 19	14 ^a <i>n</i> = 1 (2C length) activity ^b : 14 ↑ highest Mor04m ^c	3 ^a <i>n</i> = 3 (4C length) activity ^b : 3 ↓	18 ^a <i>n</i> = 6 (7C length) activity ^b : 18 ↓	13 ^a <i>n</i> = 0 (1C length) activity ^b : 13 ↓
 6, 25,26 and 27	6 ^a <i>n</i> = 0 (1C length) activity ^b : 6 ↑	6 ^a <i>n</i> = 0 (1C length) activity ^b : 6 ↑	26 ^a <i>n</i> = 2 (3C length) activity ^b : 26 ↑ highest RDF060m ^c	6 ^a <i>n</i> = 0 (1C length) activity ^b : 6 ↑ lowest R5m ^c highest HATS4p & De ^c

^a The most appropriate chain length that gives the highest activity within the same series.

^b Comparison of descriptor values and cytotoxic activity of considered compound and compound 1.

^c Comparison of descriptor values within the same series.

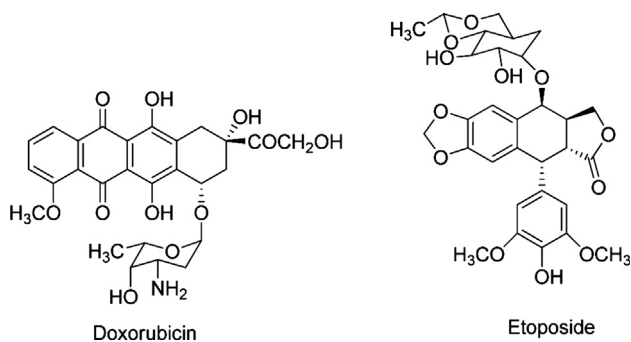


Fig. 4. Chemical structures of reference drugs.

be generated from quinone by enzymatic one-electron reduction, and/or direct reduction (non-enzymatically) via NADPH or NADH present in the cells (Fig. 5) [8,53,54].

QSAR results demonstrated that cytotoxic activities of compounds **1** and **3–36** against the investigated cell lines were influenced by distinct molecular descriptors. This indicates that such distinct chemical properties are crucial for the cytotoxic activity against particular cell lines. Particularly, atomic masses, van der Waals volume and dipole moments seemed to be important descriptors for the cytotoxic activity against cell lines that use doxorubicin as the reference drug such as HepG2, HuCCA-1 and A549 whereas the atomic polarizability was shown to be crucial for MOLT-3 that uses etoposide as the reference drug. Therefore, it could be hypothesized that the mechanism of cytotoxic activity of quinone compounds against HepG2, HuCCA-1 and A549 cells may be similar whereas that of MOLT-3 cell may act through a different mechanism of action.

Alkylation of biomolecules and ROS production have been proposed to be the main mechanisms of quinones cytotoxicity [24,56,57]. The ability of quinones to act as electrophiles contributes to alkylation mechanism whereas their ability to act as oxidants gives rise to the ROS production [57]. Quinones are highly redox active molecules and they are capable of generating ROS via redox cycles (Fig. 5) [57,59]. The ease of reduction of such compounds is expressed by their redox potentials [59]. The redox potential of quinones is correlated to their ROS production ability as well as biological activities [6,60,61] and can be modulated by

substituents on the quinone ring [59]. For example, electron-donating substituents increase electron density but decrease electrophilicity on the ring thereby impaired redox potential and ROS producing ability. In contrast, electron-withdrawing substituents affect vice versa [59]. In addition, it should be considered that the cytotoxic activity of quinones is influenced by multiple mechanisms and factors including alkylation, ROS production and pharmacokinetic properties.

It could be deduced from the QSAR analysis that chemical properties such as high atomic masses, high van der Waals volume, high electronegativity, high dipole moments and high polarizabilities are partially responsible for potent cytotoxic activity of compounds as shown in Table 12.

These chemical properties are associated with pharmacokinetic profiles, which affect the activities of compounds. Particularly, cell entry is a crucial step that allows compounds to reach the intracellular target sites of actions. Appropriate size, shape and lipophilicity of compounds are also important factors facilitating cell entry. In addition, particular conformations or isomers are required for their interaction at target sites. The QSAR analysis demonstrated that values of atomic masses-weighted, dipole moment-weighted and polarizability-weighted descriptors related to the type, size, shape, hydrocarbon chain length and position of substituents.

In summary, atomic masses, dipole moments and polarizabilities play integral roles in determining cell entry capability of compounds. That is the appropriate atomic mass refers to the appropriate size and shape of compounds that are suitable for cell entry. Dipole moments and polarizabilities may account for the charge distribution and net charge of molecules pertaining to the lipophilicity as well as the ROS production ability. Therefore, the importance of chemical and pharmacokinetic properties (as described by the selected significant descriptors) in concomitant with the mechanism of actions of reference drugs could be used in explaining the bioactivities of the investigated cell lines. Herein, the mechanism of action of doxorubicin could be applied for the explanation of QSAR analysis of HepG2, HuCCA-1 and A549 cell lines while etoposide could be used for the MOLT-3 cell line.

Doxorubicin exerted its anticancer activity via intercalation between DNA base pairs [3], stabilization of the topoisomerase II-DNA cleavage complex [29] as well as production of ROS [29,30]. Shape, size and charge distribution of compounds are important factors facilitating the two former mechanism of actions whereas the 1,4-quinone moiety accounts for the latter mechanism that is the ROS production. According to QSAR analysis, the shape and size of compounds are likely to play predominant roles in the cytotoxic activity against HepG2 and HuCCA-1 cell lines as represented by atomic masses descriptors (Mor04m, RDF050m and RDF065m) and atomic van der Waals volume ($R8v+$) as shown in Table 5. The highest value of atomic mass-weighted descriptor (Mor04m), exerts the highest cytotoxic activity against HepG2 and HuCCA-1 cell lines, as observed in trifluoroacetyl analog **32**. In addition, the high value of atomic van der Waals volume ($R8v+$) was found in analog **32** exhibiting the highest cytotoxic activity against the HepG2 cell line. It is notable that the lipophilic trifluoroacetylphenylamino moiety and the planar quinone structure of analog **32** facilitated cell entry and enhanced DNA intercalation thereby resulting in more potent activity as compared to acetyl compound **8**. It could be explained that replacement of hydrogen atoms of acetyl group (**8**) by fluorine atoms gives rise to high atomic masses and high atomic van der Waals volume as well as increased redox potential of the trifluoroacetyl analog **32**. In contrast, 1-adamantyl amino compound **21** exerted the lowest activity against the HepG2 cell line. This may be ascribed to the effect of non-planar bulky structure of the 1-adamantyl moiety that makes compound **21** unsuitable for DNA intercalation.

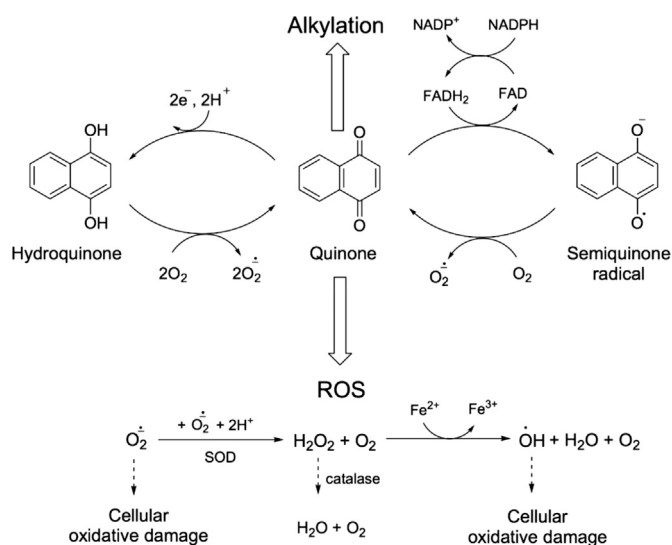


Fig. 5. Possible anticancer effect of 1,4-quinone (modified from Refs. [55–58]).

Table 12
Summary of relationships between significant descriptors and possible mechanism of actions of compounds **1** and **3–36** based on mechanism of actions of reference drugs.

Cell line	Reference drug and mechanism of action	Significant descriptors and their effects on chemical properties of compounds	Significant effects related with cytotoxic activity of compounds	Requirements of significant values of descriptor for potent cytotoxic activity
HepG2 HuCCA-1	Doxorubicin : DNA intercalation ROS production	van der Waals volume (HepG2) Atomic mass-weighted (HepG2 & HuCCA-1) • Size & Shape	Cell entry DNA intercalation	High values
A549	Doxorubicin : DNA intercalation ROS production	Dipole moment weighted • Polarity/charge Atomic mass-weighted • Size & Shape	Cell entry ROS production DNA intercalation	High values High values
MOLT-3	Etoposide: Semiquinone and ROS productions	Polarizability-weighted Electronegativity-weighted • Polarity/charge Atomic mass-weighted • Size & Shape	ROS production Cell entry	High values Low values

Furthermore, dipole moment-weighted descriptors (EEig03d and ESpm13d) play crucial roles in governing the cytotoxic effect against the A549 cell line. Compounds with high dipole moment could induce positive and negative charges on the molecule giving rise to potent cytotoxic activity as seen in trifluoroacetyl compounds **32** and **33** in which analog **32** was shown to be the most potent compound. Such potent activity of compound **32** could be attributed to the high electronegativity of fluorine atoms in the trifluoroacetyl group thereby inducing high charge distribution on the molecule as well as increasing the electrophilicity of the 1,4-quinone core structure in interacting with nucleophilic target cells. Moreover, the ROS production of 1,4-quinone compounds arises from the generated semiquinone that ultimately produced superoxide and/or hydroxyl radicals culminating in oxidative cell damage and cell death.

On the other hand, etoposide is a non-intercalative topoisomerase II poison that interacts within the enzyme active site at the DNA–enzyme interface [48,49,52]. The cytotoxic activity of etoposide is highly dependent on the redox reaction, which accounts for the production of phenoxy radical and the semiquinone toxic metabolite [29,52]. All of the studied compounds contained the 1,4-quinone moiety as the core structure (Figs. 1 and 2), which is the key pharmacophore for topoisomerase II poison activity. Therefore, it could be hypothesized that the tested compounds possibly have the same capability of inhibiting DNA unwinding *via* the production of semiquinone (Fig. 5). The QSAR analysis revealed that polarizability and electronegativity of the compound are closely related with potent cytotoxic activity against MOLT-3 cell line, as shown in QSAR equation (Table 5), in which high polarizability and high electronegativity give rise to high redox potential of the compounds thereby enhance semiquinone radical production. Particularly, the most potent *p*-amino benzoic acid analog (**29**) possessed the highest value of polarizability-weighted descriptor (HATS4p) as well as high value of electronegativity-weighted descriptor (De) as shown in Table 4. Similarly, the second most potent *p*-trifluoroacetylphenylamino compound (**33**) possessed the highest value of De and high value of HATS4p (Table 4). Furthermore, fluorine substitution on compounds **32** and **33** significantly gives rise to an increase of atomic masses-weighted descriptor (R5m) or lipophilicity which in turn weakens the cytotoxic activity (MOLT-3) as compared to their parents (**8** and **9**) as shown in Table 4. Owing to higher polarized molecules afforded higher activity, therefore, it is possible that the molecules with higher lipophilicity may impair cell entry to reach their intracellular target sites. Of the series of *p*-substituents (**9**, **12**, **29** and **33**) on phenylamino moiety, their

cytotoxic activity (MOLT-3) are governed by the polarized functional groups as the following: **29** (*p*-CO₂H) > **9** (*p*-COCH₃) > **33** (*p*-COCF₃) > **12** (*p*-NH-C₆H₅).

At this point, the findings from QSAR analyses indicate the significance of diverse substituents at specific positions that may affect the overall chemical properties as well as the pharmacokinetic profiles of compounds. A summary of the relationships between the selected significant descriptors and the possible underlying mechanisms of cytotoxic activity based on reference drugs are presented in Table 12.

3. Conclusion

A series of 1,4-naphthoquinone derivatives (**3–12**) were synthesized and investigated for their cytotoxic activity against HepG2, HuCCA-1, A549 and MOLT-3 cell lines. Novel anticancer agents such as compound **8** exhibited the most potent cytotoxic activity against HepG2, HuCCA-1 and A549 cell lines whereas compound **9** exerted the most potent activity against the MOLT-3 cell line. Interestingly, quinones **5**, **6**, **8**, and **9** displayed higher cytotoxic activity against HepG2 cell than the reference drug, etoposide. QSAR analysis demonstrated the significance of atomic masses-weighted descriptors (Mor04m, RDF050m, RDF060m and RDF065m) in the prediction of cytotoxic activity against HepG2, HuCCA-1 and A549 cell lines. Moreover, the atomic van der Waals volume (R8v+) was also deduced to be involved with the cytotoxic activity against the HepG2 cell line. In addition, dipole moments-weighted descriptors (EEig03d and ESpm13d) were also shown to be important in prediction of the cytotoxic activity against the A549 cell line. In contrast, polarizabilities-weighted descriptor (HATS4p) and electronegativities-weighted descriptor (De) influence the cytotoxic activity against the MOLT-3 cell line. The results indicated that the cytotoxic activity of such compounds against particular cell lines might arise from distinct mechanism of actions. The selected significant descriptors indicated that certain chemical properties might be relevant to pharmacokinetic profiles (i.e. cell entry and interaction at the target sites). It could be deduced that chemical properties such as size and shape, lipophilicity, polarity and charge distribution are important factors related to pharmacokinetic profiles that may enhance the cytotoxic activity. Significantly, the findings revealed the rational design of trifluoroacetyl analog (**32**) as a promising potential anticancer agent toward HepG2, HuCCA-1 and A549 cell lines while the *p*-amino benzoic acid analog (**29**) was the most potent compound against the MOLT-3 cell line.

4. Experimental section

4.1. General

Column chromatography was carried out using silica gel 60 (70–230 mesh ASTM). Analytical thin-layer chromatography (TLC) was performed with silica gel 60 F₂₅₄ aluminum sheets. ¹H and ¹³C NMR spectra were recorded on a Bruker AVANCE 300 NMR spectrophotometer (operating at 300 MHz for ¹H and 75 MHz for ¹³C). FTIR spectra were obtained using a universal attenuated total reflectance attached to a Perkin–Elmer Spectrum One spectrophotometer. High-resolution mass spectra (HRMS) were recorded on a Bruker Daltonics (microTOF). Melting points were determined using a Griffin melting point apparatus and were uncorrected. HPLC was carried out using Dionex, Ultimate 3000 equipped with UV–visible detector at 254 nm, column (Acclaim TM¹²⁰, C18, 3 μm, 120°A, 150 mm × 2.1 mm), mobile phases: 0.1% formic acid in H₂O (A) and acetonitrile (B), condition: isocratic at 95% B, flow rate 0.1 mL/min, running time 10 min, samples were prepared in acetonitrile or methanol.

Chemicals purchased from commercial suppliers were used without further purification. All biological tested compounds were >95% purity (96–100%) as determined by HPLC, except for compound **7** that showed 91% purity, **1** ≥ 98.0% (Fluka).

Reagents using in cell culture and assay were obtained from the following sources. Ham's/F12 (nutrient mixture F-12), DMEM (Dulbecco's Modified Eagle's Medium), RPMI-1640 (Rosewell Park Memorial Institute medium), FBS (fetal bovine serum) from Hyclone laboratories, USA; MTT (3-(4,5-dimethylthiazole-2-yl)-2,5-diphenyltetrazolium bromide), XTT (2,3-bis-(2-methoxy-4-nitro-5-sulphophenyl)-2H-tetrazolium-5-carboxanilide), PMS (5-methylphenazin-5-ium methyl sulfate), L-glutamine, penicillin–streptomycin, sodium pyruvate and glucose from Sigma, DMSO (dimethyl sulfoxide) from Merck.

4.2. Chemistry: general procedure

A mixture of appropriate amine **2** (5 mmol) and 2,3-dichloronaphthoquinone **1** (5 mmol) in absolute ethanol (20 mL) was stirred under reflux with stirring until completion of the reaction as monitored by TLC and then concentrated under reduced pressure. Water (20 mL) was added and extracted with EtOAc (3 × 20 mL). The organic layer was dried over anhydrous sodium sulfate, filtered and concentrated. The crude product was purified using silica gel column chromatography to afford the pure product.

4.2.1. 2-(*n*-Butylamino)-3-chloronaphthalene-1,4-dione (**3**)

Yield 51%. mp 108–110 °C (110–112 °C) [62]. IR (UATR) cm⁻¹: 3304, 1683, 1598. ¹H NMR (300 MHz, dms_o-d₆) δ 0.90 (t, *J* = 7.3 Hz, 3H, CH₃), 1.33 (sex, *J* = 7.3 Hz, 2H, CH₂CH₃), 1.59 (quin, *J* = 7.3 Hz, 2H, CH₂CH₂CH₂), 3.72 (t, *J* = 7.3 Hz, 2H, NHCH₂CH₂), 7.51 (br s, 1H, NH), 7.73 (t, *J* = 7.4 Hz, 1H, ArH), 7.82 (t, *J* = 7.5 Hz, 1H, ArH), 7.97 (d, *J* = 7.7 Hz, 2H, ArH). ¹³C NMR (75 MHz, dms_o-d₆) δ 14.2, 19.8, 33.4, 44.1, 126.3, 127.0, 130.3, 132.6, 133.1, 135.4, 145.7, 175.8, 180.7. HRMS–TOF: *m/z* [M+H]⁺ calcd for C₁₄H₁₅ClNO₂: 264.0786; found: 264.0783. Purity 98.11%.

4.2.2. 2-Chloro-3-(phenylamino)naphthalene-1,4-dione (**4**)

Yield 45%. mp 218–220 °C (210 °C) [10]. IR (UATR) cm⁻¹: 3243, 1674, 1591. ¹H NMR (300 MHz, dms_o-d₆) δ 7.10–7.35 (m, 5H, ArH), 7.81 (dt, *J* = 7.6, 1.5 Hz, 1H, ArH), 7.87 (dt, *J* = 7.6, 1.5 Hz, 1H, ArH), 8.03 (dd, *J* = 7.3, 0.9 Hz, 2H, ArH), 9.31 (s, 1H, NH). ¹³C NMR (75 MHz, dms_o-d₆) δ 124.4, 124.9, 126.6, 127.0, 128.4, 130.7, 132.4, 133.7, 135.3, 139.3, 143.6, 177.2, 180.6. HRMS–TOF: *m/z* [M+H]⁺ calcd for C₁₆H₁₁ClNO₂: 284.0473; found: 284.0472. Purity 100.00%.

4.2.3. 2-Chloro-3-(quinolin-8-ylamino)naphthalene-1,4-dione (**5**)

Yield 43%. mp 301–303 °C. IR (UATR) cm⁻¹: 3299, 1670, 1593. ¹H NMR (300 MHz, dms_o-d₆) δ 7.44–7.57 (m, 2H, ArH), 7.63 (t, *J* = 7.6 Hz, 1H, ArH), 7.72–7.90 (m, 4H, ArH), 8.16 (d, *J* = 7.5 Hz, 1H, ArH), 8.40 (d, *J* = 8.3 Hz, 1H, ArH), 8.69 (d, *J* = 4.1 Hz, 1H, ArH), 9.45 (s, 1H, NH). ¹³C NMR (75 MHz, dms_o-d₆) δ 121.8, 122.3, 124.1, 126.5, 126.7, 127.0, 128.8, 131.2, 132.2, 133.8, 135.0, 136.4, 137.1, 140.8, 146.1, 149.7, 176.9, 180.2. HRMS–TOF: *m/z* [M+H]⁺ calcd for C₁₉H₁₂ClN₂O₂: 335.0582; found: 335.0589. Purity 96.04%.

4.2.4. 2-(*N*-methyl-*N*-phenylamino)-3-chloronaphthalene-1,4-dione (**6**)

Yield 56%. mp 100–102 °C. IR (UATR) cm⁻¹: 1671, 1590. ¹H NMR (300 MHz, dms_o-d₆) δ 3.34 (s, 3H, NCH₃), 6.89 (t, *J* = 7.3 Hz, 1H, ArH), 6.95 (d, *J* = 7.8 Hz, 2H, ArH), 7.23 (t, *J* = 7.3 Hz, 2H, ArH), 7.85–8.10 (m, 4H, ArH). ¹³C NMR (75 MHz, dms_o-d₆) δ 39.7 (superimposed with dms_o-d₆ peaks), 117.1, 120.9, 126.8, 127.2, 129.3, 131.9, 132.0, 134.6, 134.7, 136.2, 146.7, 148.7, 178.4, 180.8. HRMS–TOF: *m/z* [M+H]⁺ calcd for C₁₇H₁₃ClNO₂: 298.0629; found: 298.0625. Purity 100.00%.

4.2.5. 2-(2-Chloro-1,4-dihydro-1,4-dioxonaphthalen-3-ylamino)benzoic acid (**7**)

Yield 26%. mp 240–242 °C. IR (UATR) cm⁻¹: 3302, 2925, 1677, 1653, 1605, 1567. ¹H NMR (300 MHz, dms_o-d₆) δ 7.00 (d, *J* = 8.2 Hz, 1H, ArH), 7.16 (t, *J* = 7.7 Hz, 1H, ArH), 7.55 (t, *J* = 7.2 Hz, 1H, ArH), 7.81–8.09 (m, 5H, ArH), 10.05 (s, 1H, NH). ¹³C NMR (75 MHz, dms_o-d₆) δ 118.5, 120.0, 123.2, 123.6, 126.8, 127.1, 130.8, 131.1, 132.3, 132.7, 134.0, 135.3, 140.0, 142.5, 169.3, 177.3, 180.5. HRMS–TOF: *m/z* [M+H]⁺ calcd for C₁₇H₁₁ClNO₄: 328.0371; found: 328.0384. Purity 91.07%.

4.2.6. 2-(3-Acetylphenylamino)-3-chloronaphthalene-1,4-dione (**8**)

Yield 60%. mp 205–206 °C (207–209 °C) [62]. IR (UATR) cm⁻¹: 3283, 1673, 1593. ¹H NMR (300 MHz, dms_o-d₆) δ 2.56 (s, 3H, COCH₃), 7.38 (d, *J* = 7.9 Hz, 1H, ArH), 7.46 (t, *J* = 7.6 Hz, 1H, ArH), 7.69 (s, 1H, ArH), 7.71 (d, *J* = 8.6 Hz, 1H, ArH), 7.82 (dt, *J* = 7.4, 1.4 Hz, 1H, ArH), 7.88 (dt, *J* = 7.4, 1.4 Hz, 1H, ArH), 8.05 (dd, *J* = 7.4, 1.4 Hz, 2H, ArH), 9.44 (s, 1H, NH). ¹³C NMR (75 MHz, dms_o-d₆) δ 27.2, 123.4, 124.5, 126.6, 127.0, 128.5, 128.7, 130.8, 132.4, 133.8, 135.2, 137.1, 139.8, 143.5, 177.3, 180.5, 198.1. HRMS–TOF: *m/z* [M+H]⁺ calcd for C₁₈H₁₃ClNO₃: 326.0578; found: 326.0571. Purity 97.38%.

4.2.7. 2-(4-Acetylphenylamino)-3-chloronaphthalene-1,4-dione (**9**)

Yield 61%. mp 237–238 °C. IR (UATR) cm⁻¹: 3236, 1672, 1594. ¹H NMR (300 MHz, dms_o-d₆) δ 2.59 (s, 3H, COCH₃), 7.17 (d, *J* = 8.5 Hz, 2H, ArH), 7.80–7.92 (m, 4H, ArH), 8.06 (d, *J* = 7.4 Hz, 2H, ArH), 9.55 (s, 1H, NH). ¹³C NMR (75 MHz, dms_o-d₆) δ 27.0, 122.3, 126.7, 127.1, 128.9, 131.0, 132.1, 132.2, 134.0, 135.2, 143.1, 144.2, 177.5, 180.4, 197.1. HRMS–TOF: *m/z* [M+H]⁺ calcd for C₁₈H₁₃ClNO₃: 326.0578; found: 326.0581. Purity 100.00%.

4.2.8. 2-Chloro-3-(phenethylamino)naphthalene-1,4-dione (**10**)

Yield 62%. mp 109–111 °C. IR (UATR) cm⁻¹: 3326, 1674, 1599. ¹H NMR (300 MHz, dms_o-d₆) δ 2.92 (t, *J* = 7.3 Hz, 2H, CH₂Ph), 3.96 (q, *J* = 7.1 Hz, 2H, NHCH₂), 7.16–7.32 (m, 5H, ArH), 7.50 (br s, 1H, NH), 7.73 (t, *J* = 7.5 Hz, 1H, ArH), 7.83 (t, *J* = 7.5 Hz, 1H, ArH), 7.97 (d, *J* = 7.5 Hz, 2H, ArH). ¹³C NMR (75 MHz, dms_o-d₆) δ 37.4, 45.9, 126.3, 126.8, 127.0, 128.9, 129.2, 130.4, 132.4, 133.1, 135.4, 139.0, 145.8, 175.8, 180.6. HRMS–TOF: *m/z* [M+H]⁺ calcd for C₁₈H₁₅ClNO₂: 312.0786; found: 312.0785. Purity 98.79%.

4.2.9. 2-(3,4-Dimethoxyphenethylamino)-3-chloronaphthalene-1,4-dione (**11**)

Yield 65%. mp 148–149 °C. IR (UATR) cm⁻¹: 3327, 1676, 1601. ¹H NMR (300 MHz, dms_o-d₆) δ 2.84 (t, *J* = 7.1 Hz, 2H, CH₂Ph), 3.65, 3.71

(2s, 6H, 2 × OCH₃), 3.95 (q, *J* = 7.1 Hz, 2H, NHCH₂), 6.72 (d, *J* = 8.5 Hz, 1H, ArH), 6.80 (s, 1H, ArH), 6.81 (d, *J* = 7.6 Hz, 1H, ArH), 7.37 (br t, 1H, NH), 7.73 (t, *J* = 7.4 Hz, 1H, ArH), 7.82 (t, *J* = 7.4 Hz, 1H, ArH), 7.93 (d, *J* = 7.4 Hz, 1H, ArH), 7.96 (d, *J* = 7.4 Hz, 1H, ArH). ¹³C NMR (75 MHz, dms_o-d₆) δ 36.9, 46.0, 55.8, 55.9, 112.5, 113.2, 121.3, 126.2, 126.9, 130.4, 131.4, 132.4, 133.1, 135.3, 147.9, 149.1, 175.9, 180.7. HRMS–TOF: *m/z* [M+Na]⁺ calcd for C₂₀H₁₈ClNNaO₄: 394.0817; found: 394.0823. Purity 99.51%.

4.2.10. 2-Chloro-3-[[4-(phenylamino)phenyl]amino]-naphthalene-1,4-dione (**12**)

Yield 37%. mp 196–198 °C. IR (UATR) cm⁻¹: 3342, 3295, 1670, 1595. ¹H NMR (300 MHz, dms_o-d₆) δ 6.82 (t, *J* = 7.3 Hz, 1H, ArH), 7.01–7.09 (m, 6H, ArH), 7.24 (t, *J* = 7.5 Hz, 2H, ArH), 7.79 (t, *J* = 7.4 Hz, 1H, ArH), 7.86 (t, *J* = 7.3 Hz, 1H, ArH), 8.03 (d, *J* = 7.4 Hz, 2H, ArH), 8.21, 9.24 (2s, 2H, NH). ¹³C NMR (75 MHz, dms_o-d₆) δ 116.6, 117.1, 120.1, 126.2, 126.5, 127.0, 129.7, 130.6, 131.2, 132.6, 133.4, 135.3, 141.1, 143.7, 143.9, 176.8, 180.6. HRMS–TOF: *m/z* [M+H]⁺ calcd for C₂₂H₁₆ClN₂O₂: 375.0895; found: 375.0895. Purity 99.92%.

4.3. Cytotoxic assay

The cytotoxic activity of compounds (**1** and **3–12**) against the four tested types of human cancer cell lines was performed using etoposide and doxorubicin as reference drugs. Lung carcinoma (A549) and cholangiocarcinoma (HuCCA-1) cell lines were grown in Hamm's/F12 containing 2 mM L-glutamine supplemented with 100 U/mL penicillin–streptomycin and 10% FBS. Lymphoblastic leukemia (MOLT-3) cell line was cultured in RPMI-1640 medium containing 2 mM L-glutamine, 100 U/mL penicillin–streptomycin, sodium pyruvate, glucose and 10% FBS. Hepatocellular carcinoma (HepG2) cell line was cultured in DMEM medium containing 100 U/mL penicillin–streptomycin and 10% FBS. Briefly, cell lines suspended in RPMI-1640 containing 10% FBS were seeded at a density of 5 × 10³–2 × 10⁴ cells per well in a 96-well plate (Costar No. 3599, USA) and then incubated at 37 °C under a humidified atmosphere with 95% air and 5% CO₂ for 24 h. An equal volume of additional medium containing either the serial dilutions of the tested compounds, positive control (etoposide and/or doxorubicin) or negative control (DMSO) was added to the desired final concentrations. The microtiter plates were further incubated for 48 h. Cell viability in each well was determined by staining with MTT assay [63–65] (for adherent cells: A549, HuCCA-1 and HepG2 cells) or XTT assay [66] (for suspended cells: MOLT-3 cells). The plates were read on a microplate reader (Molecular Devices, USA). The absorbance was recorded at 550 nm. Finally, IC₅₀ values were determined as the required concentration in which tested compounds afforded 50% inhibition of cell growth.

4.4. Cytotoxicity assay

Cytotoxicity was tested using normal embryonic lung cells (MRC-5). The cells were grown in DMEM medium supplemented with 100 U/mL penicillin–streptomycin and 10% FBS. The assay was performed as previously described for human cancer cells (Section 4.3). The cell viability was determined by MTT assay [63–65]. The MTT solution (10 μL/100 μL medium) was added to all wells of an assay and plates were incubated as described above for 2–4 h. Subsequently, DMSO was added to dissolve the resulting formazan by sonication. The plates were read on a microplate reader (Molecular Devices, USA) using a test wavelength of 550 nm and a reference wavelength of 650 nm. The IC₅₀ value was determined as the compound concentration that inhibited cell growth by 50%. The

compounds exhibited IC₅₀ > 50 μg/mL were considered as non-cytotoxic.

4.5. QSAR analysis

Conceptually, molecular structures of 35 compounds encompassing the tested compounds (**1** and **3–12**) and the virtually constructed compounds (**13–36**) were drawn, geometrically optimized and subjected to descriptor calculation in order to obtain values of quantum chemical and molecular descriptors. The X (descriptors) and Y (cytotoxic activity) block of data from the tested compounds (**1** and **3–12**) were further used in the development of QSAR models. Finally, the cytotoxic activities of virtual constructs (**13–36**) were calculated from the QSAR equations.

4.5.1. Data set

Eleven compounds (**1** and **3–12**) and their experimental IC₅₀ values were used in the development of QSAR models. IC₅₀ values were converted to pIC₅₀ values by taking the negative logarithm to the base of 10 (–log IC₅₀) as to obtain distribution of data points. Herein, four data sets were constructed pertaining to the cytotoxic activity against four cancer cell lines (HepG2, HuCCA-1, A549 and MOLT-3). QSAR models of the cytotoxic activity against each cell line were developed separately.

4.5.2. Molecular structure optimization and descriptor calculation

Chemical structures of a set of 35 compounds were drawn using the GaussView software [41] as shown in Figs. 1 and 2. All molecular structures were initially subjected to geometrical optimization using Gaussian 09 [67] at the semi-empirical Austin Model 1 (AM1) level followed by a subsequent density functional theory (DFT) calculation using the Becke's three-parameter hybrid method with the Lee–Yang–Parr correlation functional (B3LYP) together with the 6–31g(d) level. Geometrical optimization provided low-energy conformers in which their output files were consequently used for extracting quantum chemical descriptors using an in-house developed script. Quantum chemical descriptors consisted of the mean absolute atomic charge (*Q_m*), total energy (*E_{total}*), total dipole moment (*μ*), highest occupied molecular orbital energy (*E_{HOMO}*), lowest unoccupied molecular orbital energy (*E_{LUMO}*), energy difference of HOMO and LUMO (HOMO–LUMO_{Gap}), electron affinity (EA), ionization potential (IP), Mulliken electronegativity (*χ*), hardness (*η*), softness (*S*), electrophilic index (*ω_i*) and electrophilicity (*ω*). Dragon software (version 5.5) [42] was used for further calculation of an additional set of 3224 molecular descriptors using the aforementioned low-energy molecular structures from B3LYP/6-31g(d) calculation as input data. Dragon descriptors can be categorized into the following 22 classes as follows: Constitutional descriptors, Topological descriptors, Walk and path counts, Connectivity indices, Information indices, 2D autocorrelation, Edge adjacency indices, Burden eigenvalues, Topological charge indices, Eigenvalue-based indices, Randic molecular profiles, Geometrical descriptors, RDF descriptors, 3D-Morse descriptors, WHIM descriptors, GETAWAY descriptors, Functional group counts, Atom-centered fragments, Charge descriptors, Molecular properties, 2D binary fingerprints and 2D frequency fingerprints.

4.5.3. Descriptor selection

All quantum chemical and molecular descriptors of the experimentally tested compounds (**1** and **3–12**) were used as input data for descriptor selection using Monte Carlo or correlation-based approaches.

The starting set of descriptors consisted of 13 quantum chemical descriptors and 3224 molecular descriptors and important

descriptors were identified by a Monte Carlo approach [68] coupled to Multiple Linear Regression (MC–MLR) using an in-house developed script.

Prior to performing MC–MLR, constant and insignificant descriptors were initially removed whose standard deviation is less than 0.1. Remaining descriptors were standardized and correlation coefficients between descriptor pairs were calculated. Any pair of descriptor whose correlation coefficient is greater than 0.9 were considered as highly correlated and was removed. The same process was repeated until there were no redundant or highly correlated descriptors.

Correlation-based feature selection was initially performed by calculating the pair-correlation of each descriptor value and bioactivity (pIC_{50}). Threshold value of correlation coefficient (r) of 0.6 was used as the cut off. Descriptors representing $|r| < 0.6$ were considered as low correlated descriptor and were discarded from this study. The remaining descriptors along with the pIC_{50} value were used as input data for further feature selection by stepwise MLR regression as implemented in SPSS statistics 18.0 (SPSS Inc., USA).

4.5.4. Multivariate analysis using multiple linear regression

Selected descriptors were used as independent variables and pIC_{50} values were used as the dependent variable for multivariate analysis by Waikato Environment for Knowledge Analysis (WEKA) version 3.4.5 [69] using MLR.

Constructed MLR models are summarized according to the following equation:

$$Y = B_0 + \sum B_n X_n \quad (1)$$

where Y is the pIC_{50} values of compounds, B_0 is the intercept and B_n are the regression coefficient of descriptors X_n .

4.5.5. Data sampling

The data set was divided into 2 subsets comprising of the training set and the testing set and such data divisions were performed by means of leave-one-out cross validation (LOO-CV). In brief, one sample was excluded and used as the testing set while the remaining $N - 1$ samples were used as the training set. The process was repeated until every sample in the data set was used as the testing set to predict the Y variable.

4.5.6. Outlier detection

Outliers were detected when the standardized differences between actual and predicted values (i.e. the residual) are greater than ± 2 . Standardization of residuals was calculated as following equation:

$$X_{ij}^{\text{stn}} = (X_{ij} - \bar{X}_j) / \sqrt{\sum_{i=1}^N (x_{ij} - \bar{X}_j)^2 / N} \quad (2)$$

where X_{ij}^{stn} is the standardized value, is the value of each sample, is the mean of each descriptors and N is the sample size of the data set. Identified outliers were subjected to removal from the model.

4.5.7. Evaluating the performance of QSAR models

The performance of QSAR models was evaluated by statistical parameters comprising of correlation coefficient (R) and the root mean square error (RMSE) which represented the predictive performance and predictive error of the models, respectively.

4.5.8. Prediction of structurally modified compounds (13–36) using QSAR models

Equations obtained from QSAR analysis in concomitant with molecular descriptors obtained from Gaussian and Dragon calculated were used in computing the predicted pIC_{50} values of 24 virtually constructed compounds (13–36) against the four tested cancer cell lines.

Acknowledgment

This project is supported by the Office of the Higher Education Commission, Mahidol University under the National Research Universities Initiative and Annual Government Grant under Mahidol University (2556–2558 B.E.). We appreciate Miss Sasiwimon Lalitmanat and Dr. Thummaruk Suksrichavalit for performing HPLC analysis of the compounds. We gratefully acknowledge The Chulabhorn Research Institute for cytotoxic testings.

Appendix A. Supplementary data

Supplementary data related to this article can be found online at <http://dx.doi.org/10.1016/j.ejmech.2014.07.024>. These data include MOL files and InChIKeys of the compounds described in this article.

References

- [1] T. Vos, A.D. Flaxman, M. Naghavi, R. Lozano, C. Michaud, M. Ezzati, K. Shibuya, J.A. Salomon, S. Abdalla, V. Aboyans, J. Abraham, I. Ackerman, R. Aggarwal, S.Y. Ahn, M.K. Ali, M. Alvarado, H.R. Anderson, L.M. Anderson, K.G. Andrews, C. Atkinson, L.M. Baddour, A.N. Bahalim, S. Barker-Collo, L.H. Barrero, D.H. Bartels, M.G. Basanez, A. Baxter, M.L. Bell, E.J. Benjamin, D. Bennett, E. Bernabe, K. Bhalla, B. Bhandari, B. Bikbov, A. Bin Abdulhak, G. Birbeck, J.A. Black, H. Blencowe, J.D. Blore, F. Blyth, I. Bolliger, A. Bonaventure, S. Boufous, R. Bourne, M. Boussinesq, T. Braithwaite, C. Brayne, L. Bridgett, S. Brooker, P. Brooks, T.S. Brugha, C. Bryan-Hancock, C. Bucello, R. Buchbinder, G. Buckle, C.M. Budke, M. Burch, P. Burney, R. Burstein, B. Calabria, B. Campbell, C.E. Canter, H. Carabin, J. Carapetis, L. Carmona, C. Cella, F. Charlson, H. Chen, A.T. Cheng, D. Chou, S.S. Chugh, L.E. Coffeng, S.D. Colan, S. Colquhoun, K.E. Colson, J. Condon, M.D. Connor, L.T. Cooper, M. Corriere, M. Cortinovis, K.C. de Vaccaro, W. Couser, B.C. Cowie, M.H. Criqui, M. Cross, K.C. Dabhadkar, M. Dahiya, N. Dahodwala, J. Damsere-Derry, G. Danaei, A. Davis, D. De Leo, L. Degenhardt, R. Dellavalle, A. Delossantos, J. Denenberg, S. Derrett, D.C. Des Jarlais, S.D. Dharmaratne, M. Dherani, C. Diaz-Torne, H. Dolk, E.R. Dorsey, T. Driscoll, H. Duber, B. Ebel, K. Edmond, A. Elbaz, S.E. Ali, H. Erskine, P.J. Erwin, P. Espindola, S.E. Ewoigbokhan, F. Farzadfar, V. Feigin, D.T. Felson, A. Ferrari, C.P. Ferri, E.M. Fevre, M.M. Finucane, S. Flaxman, L. Flood, K. Foreman, M.H. Forouzanfar, F.G. Fowkes, R. Franklin, M. Fransen, M.K. Freeman, B.J. Gabbe, S.E. Gabriel, E. Gakidou, H.A. Ganatra, B. Garcia, F. Gaspari, R.F. Gillum, G. Gmel, R. Gosselin, R. Grainger, J. Groeger, F. Guillemin, D. Gunnell, R. Gupta, J. Haagsma, H. Hagan, Y.A. Halasa, W. Hall, D. Haring, J.M. Haro, J.E. Harrison, R. Havmoeller, R.J. Hay, H. Higashi, C. Hill, B. Hoen, H. Hoffman, P.J. Hotez, D. Hoy, J.J. Huang, S.E. Ibeanusi, K.H. Jacobsen, S.L. James, D. Jarvis, R. Jasrasaria, S. Jayaraman, N. Johns, J.B. Jonas, G. Karthikeyan, N. Kassebaum, N. Kawakami, A. Keren, J.P. Khoo, C.H. King, L.M. Knowlton, O. Kobusingye, A. Koranteng, R. Krishnamurthi, R. Lalloo, L.L. Laslett, T. Lathlean, J.L. Leasher, Y.Y. Lee, J. Leigh, S.S. Lim, E. Limb, J.K. Lin, M. Lipnick, S.E. Lipshultz, W. Liu, M. Loane, S.L. Ohno, R. Lyons, J. Ma, J. Mabwajana, M.F. MacIntyre, R. Malekzadeh, L. Mallinger, S. Manivannan, W. Marcenes, L. March, D.J. Margolis, G.B. Marks, R. Marks, A. Matsumori, R. Matzopoulos, B.M. Mayosi, J.H. McAnulty, M.M. McDermott, N. McGill, J. McGrath, M.E. Medina-Mora, M. Meltzer, G.A. Mensah, T.R. Merriman, A.C. Meyer, V. Miglioli, M. Miller, T.R. Miller, P.B. Mitchell, A.O. Mocumbi, T.E. Moffitt, A.A. Mokdad, L. Monasta, M. Montico, M. Moradi-Lakeh, A. Moran, L. Morawska, R. Mori, M.E. Murdoch, M.K. Mwaniki, K. Naidoo, M.N. Nair, L. Naldi, K.M. Narayan, P.K. Nelson, R.G. Nelson, M.C. Nevitt, C.R. Newton, S. Nolte, P. Norman, R. Norman, M. O'Donnell, S. O'Hanlon, C. Olives, S.B. Omer, K. Ortblad, R. Osborne, D. Ozgediz, A. Page, B. Pahari, J.D. Pandian, A.P. Rivero, S.B. Patten, N. Pearce, R.P. Padilla, F. Perez-Ruiz, N. Perico, K. Pesudovs, D. Phillips, M.R. Phillips, K. Pierce, S. Pion, G.V. Polanczyk, S. Polinder, C.A. Pope 3rd, S. Popova, E. Porrini, F. Pourmalek, M. Prince, R.L. Pullan, K.D. Ramaiah, D. Ranganathan, H. Razavi, M. Regan, J.T. Rehm, D.B. Rein, G. Remuzzi, K. Richardson, F.P. Rivara, T. Roberts, C. Robinson, F.R. De Leon, L. Ronfani, R. Room, L.C. Rosenfeld, L. Rushton, R.L. Sacco, S. Saha, U. Sampson, L. Sanchez-Riera, E. Sanman, D.C. Schwebel, J.G. Scott, M. Segui-Gomez, S. Shahrzad, D.S. Shepard, H. Shin, R. Shivakoti, D. Singh, G.M. Singh, J.A. Singh, J. Singleton, D.A. Sleet, K. Sliwa, E. Smith, J.L. Smith, N.J. Stapelberg, A. Steer, T. Steiner, W.A. Stolk, L.J. Stovner, C. Sudfeld, S. Syed, G. Tamburlini,

- M. Tavakkoli, H.R. Taylor, J.A. Taylor, W.J. Taylor, B. Thomas, W.M. Thomson, G.D. Thurston, I.M. Tleyjeh, M. Tonelli, J.A. Towbin, T. Truelsen, M.K. Tsilimbaris, C. Ubeda, E.A. Undurraga, M.J. van der Werf, J. van Os, M.S. Vavilala, N. Venketasubramanian, M. Wang, W. Wang, K. Watt, D.J. Weatherall, M.A. Weinstock, R. Weintraub, M.G. Weisskopf, M.M. Weissman, R.A. White, H. Whiteford, S.T. Wiersma, J.D. Wilkinson, H.C. Williams, S.R. Williams, E. Witt, F. Wolfe, A.D. Woolf, S. Wulf, P.H. Yeh, A.K. Zaidi, Z.J. Zheng, D. Zonies, A.D. Lopez, C.J. Murray, M.A. AlMazroa, Z.A. Memish, Years lived with disability (YLDs) for 1160 sequelae of 289 diseases and injuries 1990–2010: a systematic analysis for the global burden of disease study 2010, *Lancet* 380 (2012) 2163–2196.
- [2] R.P. Verma, Anti-cancer activities of 1,4-naphthoquinones: a QSAR study, *Anticancer. Agents. Med. Chem.* 6 (2006) 489–499.
- [3] A.K. McClendon, N. Osheroff, DNA topoisomerase II, genotoxicity, and cancer, *Mutat. Res. Fundam. Mol. Mech. Mutagen* 623 (2007) 83–97.
- [4] H.R. Lawrence, A. Kazi, Y. Luo, R. Kendig, Y. Ge, S. Jain, K. Daniel, D. Santiago, W.C. Guida, S.M. Sebti, Synthesis and biological evaluation of naphthoquinone analogs as a novel class of proteasome inhibitors, *Bioorg. Med. Chem.* 18 (2010) 5576–5592.
- [5] V.K. Tandon, H.K. Maurya, A. Tripathi, G.B. ShivaKeshava, P.K. Shukla, P. Srivastava, D. Panda, 2,3-Disubstituted-1,4-naphthoquinones, 12H-benzo[b]phenothiazine-6,11-diones and related compounds: synthesis and biological evaluation as potential antiproliferative and antifungal agents, *Eur. J. Med. Chem.* 44 (2009) 1086–1092.
- [6] E.H. da Cruz, C.M. Hussene, G.G. Dias, E.B. Diogo, I.M. de Melo, B.L. Rodrigues, M.G. da Silva, W.O. Valenca, C.A. Camara, R.N. de Oliveira, Y.G. de Paiva, M.O. Goulart, B.C. Cavalcanti, C. Pessoa, E.N. da Silva Junior, 1,2,3-Triazole-, arylamino- and thio-substituted 1,4-naphthoquinones: potent antitumor activity, electrochemical aspects, and bioisosteric replacement of C-ring-modified lapachones, *Bioorg. Med. Chem.* 22 (2014) 1608–1619.
- [7] H.R. Nasiri, M.G. Madej, R. Panisch, M. Lafontaine, J.W. Bats, C.R. Lancaster, H. Schwalbe, Design, synthesis, and biological testing of novel naphthoquinones as substrate-based inhibitors of the quinol/fumarate reductase from *Wolinetella succinogenes*, *J. Med. Chem.* 56 (2013) 9530–9541.
- [8] D. Bhasin, S.N. Chettiar, J.P. Etter, M. Mok, P.K. Li, Anticancer activity and SAR studies of substituted 1,4-naphthoquinones, *Bioorg. Med. Chem.* 21 (2013) 4662–4669.
- [9] C.-K. Ryu, D.-H. Kim, The synthesis and antimicrobial activities of some 1,4-naphthoquinones (II), *Arch. Pharm. Res.* 15 (1992) 263–268.
- [10] V.K. Tandon, H.K. Maurya, N.N. Mishra, P.K. Shukla, Design, synthesis and biological evaluation of novel nitrogen and sulfur containing hetero-1,4-naphthoquinones as potent antifungal and antibacterial agents, *Eur. J. Med. Chem.* 44 (2009) 3130–3137.
- [11] J.J. Inbaraj, C.F. Chignell, Cytotoxic action of juglone and plumbagin: a mechanistic study using HaCaT keratinocytes, *Chem. Res. Toxicol.* 17 (2004) 55–62.
- [12] S.T. Huang, H.S. Kuo, C.L. Hsiao, Y.L. Lin, Efficient synthesis of 'redox-switched' naphthoquinone thiol-crown ethers and their biological activity evaluation, *Bioorg. Med. Chem.* 10 (2002) 1947–1952.
- [13] V.K. Tandon, R.B. Chhor, R.V. Singh, S. Rai, D.B. Yadav, Design, synthesis and evaluation of novel 1,4-naphthoquinone derivatives as antifungal and anticancer agents, *Bioorg. Med. Chem. Lett.* 14 (2004) 1079–1083.
- [14] K. Sasaki, H. Abe, F. Yoshizaki, In vitro antifungal activity of naphthoquinone derivatives, *Biol. Pharm. Bull.* 25 (2002) 669–670.
- [15] V.K. Tandon, D.B. Yadav, H.K. Maurya, A.K. Chaturvedi, P.K. Shukla, Design, synthesis, and biological evaluation of 1,2,3-trisubstituted-1,4-dihydrobenzo[g]quinoxaline-5,10-diones and related compounds as antifungal and antibacterial agents, *Bioorg. Med. Chem.* 14 (2006) 6120–6126.
- [16] V.K. Tandon, R.V. Singh, S. Rai, R.B. Chhor, Z.K. Khan, Synthesis and pharmacological studies of some 2-t-amino and 2,3-di-t-amino substituted 1,4-naphthoquinones and related compounds, *Boll. Chim. Farm.* 141 (2002) 304–310.
- [17] T.V. Iliina, E.A. Semenova, T.R. Pronyaeva, A.G. Pokrovskii, I.V. Nechepurenko, E.E. Shults, O.I. Andreeva, S.N. Kochetkov, G.A. Tolstikov, Inhibition of HIV-1 reverse transcriptase by aryl-substituted naphtho- and anthraquinones, *Dokl. Biochem. Biophys.* 382 (2002) 56–59.
- [18] A.J.M. Da Silva, C.D. Buarque, F.V. Brito, L. Aurelian, L.F. Macedo, L.H. Malkas, R.J. Hickey, D.V.S. Lopes, F. Noël, Y.L.B. Murakami, N.M.V. Silva, P.A. Melo, R.R.B. Caruso, N.G. Castro, P.R.R. Costa, Synthesis and preliminary pharmacological evaluation of new (\pm) 1,4-naphthoquinones structurally related to lapachol, *Bioorg. Med. Chem.* 10 (2002) 2731–2738.
- [19] G.Y. Song, Y. Kim, Y.J. You, H. Cho, S.H. Kim, D.E. Sok, B.Z. Ahn, Naphthazarin derivatives (VI): synthesis, inhibitory effect on DNA topoisomerase I and antiproliferative activity of 2- or 6-(1-oxyminoalkyl)-5,8-dimethoxy-1,4-naphthoquinones, *Arch. Pharm.* 333 (2000) 87–92.
- [20] J.C. Lien, L.J. Huang, C.M. Teng, J.P. Wang, S.C. Kuo, Synthesis of 2-alkoxy 1,4-naphthoquinone derivatives as antiplatelet, antiinflammatory, and anti-allergic agents, *Chem. Pharm. Bull.* 50 (2002) 672–674.
- [21] Y.R. Jin, C.K. Ryu, C.K. Moon, M.R. Cho, Y.P. Yun, Inhibitory effects of J78, a newly synthesized 1,4-naphthoquinone derivative, on experimental thrombosis and platelet aggregation, *Pharmacology* 70 (2004) 195–200.
- [22] D.Y. Yuk, C.K. Ryu, J.T. Hong, K.H. Chung, W.S. Kang, Y. Kim, H.S. Yoo, M.K. Lee, C.K. Lee, Y.P. Yun, Antithrombotic and antiplatelet activities of 2-chloro-3-[4-(ethylcarboxy)-phenyl]-amino-1,4-naphthoquinone (NQ12), a newly synthesized 1,4-naphthoquinone derivative, *Biochem. Pharmacol.* 60 (2000) 1001–1008.
- [23] L. Salmon-Chemin, E. Buisine, V. Yardley, S. Kohler, M.A. Debrey, V. Landry, C. Sergheraert, S.L. Croft, R.L. Krauth-Siegel, E. Davioud-Charvet, 2- and 3-Substituted 1,4-naphthoquinone derivatives as subversive substrates of trypanothione reductase and lipoamide dehydrogenase from *Trypanosoma cruzi*: synthesis and correlation between redox cycling activities and in vitro cytotoxicity, *J. Med. Chem.* 44 (2001) 548–565.
- [24] P.J. O'Brien, Molecular mechanisms of quinone cytotoxicity, *Chem. Biol. Interact.* 80 (1991) 1–41.
- [25] J. Benites, J.A. Valderrama, K. Bettega, R.C. Pedrosa, P.B. Calderon, J. Verrax, Biological evaluation of donor-acceptor aminonaphthoquinones as antitumor agents, *Eur. J. Med. Chem.* 45 (2010) 6052–6057.
- [26] T. Schneider, Y. Muthukumar, B. Hinkelmann, R. Franke, M. Doring, C. Jacob, F. Sasse, Deciphering intracellular targets of organochalcogen based redox catalysts, *Med. Chem. Commun.* 3 (2012) 784–787.
- [27] V.K. Tandon, D.B. Yadav, R.V. Singh, M. Vaish, A.K. Chaturvedi, P.K. Shukla, Synthesis and biological evaluation of novel 1,4-naphthoquinone derivatives as antibacterial and antiviral agents, *Bioorg. Med. Chem. Lett.* 15 (2005) 3463–3466.
- [28] S. Salunke-Gawali, O. Pawar, M. Nikalje, R. Patil, T. Weyhermüller, V.G. Puranik, V. Badireenath Konkimalla, Synthesis, characterization and molecular structures of homologated analogs of 2-bromo-3-(n-alkylamino)-1,4-naphthoquinone, *J. Mol. Struct.* 1056–1057 (2014) 97–103.
- [29] C. Avendaño, J.C. Menéndez, DNA intercalators and topoisomerase inhibitors, in: *Medicinal Chemistry of Anticancer Drugs*, Elsevier, Oxford, 2008, pp. 199–228.
- [30] K.R. Hande, Topoisomerase II inhibitors, *Update Cancer Ther.* 3 (2008) 13–26.
- [31] C. Nantasenamat, C. Isarankura-Na-Ayudhya, V. Prachayasittikul, Advances in computational methods to predict the biological activity of compounds, *Expert Opin. Drug Discov.* 5 (2010) 633–654.
- [32] C. Nantasenamat, C. Isarankura-Na-Ayudhya, T. Naenna, V. Prachayasittikul, A practical overview of quantitative structure-activity relationship, *Excli J.* 8 (2009) 74–88.
- [33] A. Worachartcheewan, C. Nantasenamat, C. Isarankura-Na-Ayudhya, V. Prachayasittikul, QSAR study of amidino bis-benzimidazole derivatives as potent anti-malarial agents against *Plasmodium falciparum*, *Chem. Zvesti* 67 (2013) 1462–1473.
- [34] A. Worachartcheewan, C. Nantasenamat, C. Isarankura-Na-Ayudhya, V. Prachayasittikul, Predicting antimicrobial activities of benzimidazole derivatives, *Med. Chem. Res.* (2013) 1–13.
- [35] A. Worachartcheewan, S. Prachayasittikul, R. Pingaew, C. Nantasenamat, T. Tantimongcolwat, S. Ruchirawat, V. Prachayasittikul, Antioxidant, cytotoxicity, and QSAR study of 1-adamantylthio derivatives of 3-picoline and phenylpyridines, *Med. Chem. Res.* 21 (2012) 3514–3522.
- [36] C. Hansch, A. Leo, S.B. Mekepati, A. Kurup, QSAR and ADME, *Bioorg. Med. Chem.* 12 (2004) 3391–3400.
- [37] E. Pérez-Sacau, R.G. Díaz-Peñate, A. Estévez-Braun, A.G. Ravelo, J.M. García-Castellano, L. Pardo, M. Campillo, Synthesis and pharmacophore modeling of naphthoquinone derivatives with cytotoxic activity in human promyelocytic leukemia HL-60 cell line, *J. Med. Chem.* 50 (2007) 696–706.
- [38] W.R. Leopold, J.L. Shillis, A.E. Mertus, J.M. Nelson, B.J. Roberts, R.C. Jackson, Anticancer activity of the structurally novel antibiotic CI-920 and its analogues, *Cancer Res.* 44 (1984) 1928–1932.
- [39] K.M. Tewey, G.L. Chen, E.M. Nelson, L.F. Liu, Intercalative antitumor drugs interfere with the breakage-reunion reaction of mammalian DNA topoisomerase II, *J. Biol. Chem.* 259 (1984) 9182–9187.
- [40] J.W. Lown, S.K. Sim, K.C. Majumdar, R.Y. Chang, Strand scission of DNA by bound adriamycin and daunorubicin in the presence of reducing agents, *Biochem. Biophys. Res. Commun.* 76 (1977) 705–710.
- [41] I.I.R. Dennington, T. Keith, J. Millam, K. Eppinnett, W.L. Hovell, R. Gilliland, GaussView, Version 3.09, Semicem Shawnee Mission, KS, USA, 2003.
- [42] Talete, Dragon for Windows (Software for Molecular Descriptor Calculations), Version 5.5, Milan, Italy, 2007.
- [43] R.P. Verma, C. Hansch, Elucidation of structure-activity relationships for 2- or 6-substituted-5,8-dimethoxy-1,4-naphthoquinones, *Bioorg. Med. Chem.* 12 (2004) 5997–6009.
- [44] N. Osheroff, Eukaryotic topoisomerase II. Characterization of enzyme turnover, *J. Biol. Chem.* 261 (1986) 9944–9950.
- [45] J.C. Wang, DNA topoisomerases, *Annu. Rev. Biochem.* 65 (1996) 635–692.
- [46] J.C. Wang, Cellular roles of DNA topoisomerases: a molecular perspective, *Nat. Rev. Mol. Cell Biol.* 3 (2002) 430–440.
- [47] J.J. Champoux, DNA topoisomerases: structure, function, and mechanism, *Annu. Rev. Biochem.* 70 (2001) 369–413.
- [48] J.M. Fortune, N. Osheroff, Topoisomerase II as a target for anticancer drugs: when enzymes stop being nice, *Prog. Nucleic Acid Res. Mol. Biol.* 64 (2000) 221–253.
- [49] A.M. Wilstermann, N. Osheroff, Stabilization of eukaryotic topoisomerase II-DNA cleavage complexes, *Curr. Top. Med. Chem.* 3 (2003) 321–338.
- [50] S.H. Kaufmann, Cell death induced by topoisomerase-targeted drugs: more questions than answers, *Biochim. Biophys. Acta.* 1400 (1998) 195–211.
- [51] T.G. Gantchev, D.J. Hunting, The ortho-quinone metabolite of the anticancer drug etoposide (VP-16) is a potent inhibitor of the topoisomerase II/DNA cleavable complex, *Mol. Pharmacol.* 53 (1998) 422–428.

- [52] D.A. Jacob, S.L. Mercer, N. Osheroff, J.E. Deweese, Etoposide quinone is a redox-dependent topoisomerase II poison, *Biochemistry* 50 (2011) 5660–5667.
- [53] A. Hakura, H. Mochida, Y. Tsutsui, K. Yamatsu, Mutagenicity and cytotoxicity of naphthoquinones for Ames Salmonella tester strains, *Chem. Res. Toxicol.* 7 (1994) 559–567.
- [54] H. Soedjak, J. Hajdu, J.D. Raffetto, R. Cano, B.L. Bales, L.S. Prasad, L.D. Kispert, The structure of streptonigrin semiquinone in solution, *Biochim. Biophys. Acta.* 1335 (1997) 73–90.
- [55] S.L. de Castro, F.S. Emery, E.N. da Silva Júnior, Synthesis of quinoidal molecules: strategies towards bioactive compounds with an emphasis on lapachones, *Eur. J. Med. Chem.* 69 (2013) 678–700.
- [56] E.A. Hillard, F.C. de Abreu, D.C. Ferreira, G. Jaouen, M.O. Goulart, C. Amatore, Electrochemical parameters and techniques in drug development, with an emphasis on quinones and related compounds, *Chem. Commun. (Camb.)* (2008) 2612–2628.
- [57] J.L. Bolton, M.A. Trush, T.M. Penning, G. Dryhurst, T.J. Monks, Role of quinones in toxicology, *Chem. Res. Toxicol.* 13 (2000) 135–160.
- [58] T.J. Monks, R.P. Hanzlik, G.M. Cohen, D. Ross, D.G. Graham, Quinone chemistry and toxicity, *Toxicol. Appl. Pharmacol.* 112 (1992) 2–16.
- [59] Y. Song, G.R. Buettner, Thermodynamic and kinetic considerations for the reaction of semiquinone radicals to form superoxide and hydrogen peroxide, *Free Radic. Biol. Med.* 49 (2010) 919–962.
- [60] M.O.F. Goulart, C.L. Zani, J. Tonholo, L.R. Freitas, F.C. De Abreu, A.B. Oliveira, D.S. Raslan, S. Starling, E. Chiari, Trypanocidal activity and redox potential of heterocyclic- and 2-hydroxy-naphthoquinones, *Bioorg. Med. Chem. Lett.* 7 (1997) 2043–2048.
- [61] L. Bouffier, I. Gosse, M. Demeunynck, P. Mailley, Electrochemistry and bioactivity relationship of 6-substituted-4H-pyrido[4,3,2-kl]acridin-4-one anti-tumor drug candidates, *Bioelectrochemistry.* 88 (2012) 103–109.
- [62] R. Parr, J. Reiss, N-Substituted enamines from 3-aminobutenoic acids and 1,4-naphthoquinones, *Aust. J. Chem.* 37 (1984) 389–394.
- [63] T. Mosmann, Rapid colorimetric assay for cellular growth and survival: application to proliferation and cytotoxicity assays, *J. Immunol. Methods.* 65 (1983) 55–63.
- [64] H. Tominaga, M. Ishiyama, F. Ohseto, K. Sasamoto, T. Hamamoto, K. Suzuki, M. Watanabe, A water-soluble tetrazolium salt useful for colorimetric cell viability assay, *Anal. Commun.* 36 (1999) 47–50.
- [65] J. Carmichael, W.G. DeGraff, A.F. Gazdar, J.D. Minna, J.B. Mitchell, Evaluation of a tetrazolium-based semiautomated colorimetric assay: assessment of radiosensitivity, *Cancer Res.* 47 (1987) 936–942.
- [66] A. Doyly, J.B. Griffiths, *Mammalian Cell Culture-essential Techniques*, John Wiley and Sons Chichester, New York, Weinheim, Brisbane, Toronto, 1997.
- [67] M.J. Frisch, G.W. Trucks, H.B. Schlegel, G.E. Scuseria, M.A. Robb, J.R. Cheeseman, G. Scalmani, V. Barone, B. Mennucci, G.A. Petersson, H. Nakatsuji, M. Caricato, X. Li, H.P. Hratchian, A.F. Izmaylov, J. Bloino, G. Zheng, J.L. Sonnenberg, M. Hada, M. Ehara, K. Toyota, R. Fukuda, J. Hasegawa, M. Ishida, T. Nakajima, Y. Honda, O. Kitao, H. Nakai, T. Vreven, J.A. M. Jr., J.E. Peralta, F. Ogliaro, M. Bearpark, J.J. Heyd, E. Brothers, K.N. Kudin, V.N. Staroverov, R. Kobayashi, J. Normand, K. Raghavachari, A. Rendell, J.C. Burant, S.S. Iyengar, J. Tomasi, M. Cossi, N. Rega, J.M. Millam, M. Klene, J.E. Knox, J.B. Cross, V. Bakken, C. Adamo, J. Jaramillo, R. Gomperts, R.E. Stratmann, O. Yazyev, A.J. Austin, R. Cammi, C. Pomelli, J.W. Ochterski, R.L. Martin, K. Morokuma, V.G. Zakrzewski, G.A. Voth, P. Salvador, J.J. Dannenberg, S. Dapprich, A.D. Daniels, Ö Farkas, J.B. Foresman, J.V. Ortiz, J. Cioslowski, D.J. Fox, Gaussian Inc., Wallingford CT, 2009.
- [68] M. Hall, Correlation Based Feature Selection for Machine Learning (Doctoral dissertation), Department of Computer Science, University of Waikato, 1999.
- [69] I.H. Witten, E. Frank, M.A. Hall, *Data Mining: Practical Machine Learning Tools and Techniques*, second ed., Morgan Kaufmann, San Francisco, 2011.